Geomorphic analysis of 35 ephemeral river reaches with variable channel morphologies in the South Coast, California, USA.

By

XAVIER ROJAS NOGUEIRA

THESIS

Submitted in partial satisfaction of the requirements for the degree of

MASTER OF SCIENCE

in

HYDROLOGIC SCIENCE

in the

OFFICE OF GRADUATE STUDIES

of the

UNIVERSITY OF CALIFORNIA

DAVIS

Approved:

Chair's Name, Chair (or Co-Chair)

Member's Name

Member's Name

Committee in Charge

2022

Abstract

During the last decade, 1-m resolution topo-bathymetric digital elevation models (DEMs) have become increasingly utilized within fluvial geomorphology, but most meter-scale geomorphic analyses have only been conducted on one to a small handful of river reaches. While such analyses have contributed greatly to our collective understanding of river discharge-topography interactions, which is applicable in both river restoration design and environmental flow regulation contexts, their generalizability across a range of river types remained largely unevaluated. This study assessed the dominance of a single hydro-morphodynamic mechanism, flow convergence routing, in 35 ephemeral rivers divided among 5 channel types in California's South Coast region. To do so, we conducted geomorphic covariance structure (GCS) analysis on longitudinal standardized width (Ws) and standardized, detrended bed elevation (Zs) spatial series from 1-m resolution DEMs to explore the stage-dependent nature of fluvial landforms. We compared and contrasted results among different river types and found that in all river types there are coherent, multi-scalar structures of longitudinal fluvial topography. We find that width undulation driven flow convergence routing is a broadly relevant channel altering mechanism, however, it’s relationship with water stage height differs between river types. For example, in partly confined riffle-pool rivers, resilient width undulations at a bankfull discharge appear to control the degree to which riffle-pool morphology is self-maintaining. But in mountainous confined river reaches, width’s relationship with inferred sedimentary dynamics increases somewhat linearly with water stage height, potentially as a function of the sediment size distribution.

1 Introduction

River type classification relies on the concept that each assemblage of geomorphic processes produces a characteristic fluvial morphology (Thornbury, 1954; Kasprak et al., 2016). Yet studies investigating the relative role of a hydro-morphodynamic process across a range of different river types are lacking. For example, one might wonder if knickpoint migration is equally important for plane-bed, riffle-pool, step-pool, cascade, and bedrock river types and of equal importance in any one type across all discharges? The process could instead be meander migration, freeze-thaw bank erosion, avulsion, flow convergence routing, nonfluvial boulder emplacement, particle queuing, or dozens of others. While river pattern classifications often use numerical thresholds to delineate broad patterns (e.g., Eaton et al., 2010), albeit with some skepticism (Carson, 1984), reach-scale river classifications rarely use them.

A key limiting factor in evaluating how a hydro-morphodynamic process varies among river types has been the lack of sufficiently detailed (i.e., 1-m resolution) topo-bathymetric mapping of rivers to characterize the essential patterns of variability that drive and indicate individual morphodynamic processes. Variability is present in many key factors, such as sediment facies, aquatic and riparian vegetation, large bed elements (including wood, boulder and bedrock features), and topography. One-meter resolution topo-bathymetric digital elevation models (DEMs) are increasingly available and utilized in fluvial geomorphology (Piegay et al., 2015) to describe topography (Notebaert et al., 2009; Scown et al., 2015), segment rivers (Nardini et al., 2020), model

two-dimensional (2D) hydraulics (Pasternack, 2011), classify and mapping landforms (Cavalli et al., 2008; Clubb et al, 2017), document sedimentary dynamics (Baartman et al., 2013), identify periodic width (W) and detrended bed elevation (Zd) undulations (Brown & Pasternack, 2017; Duffin et al., 2021), and evaluating topography for specific hydro-morphodynamic mechanisms (Pasternack et al., 2018a, b; Pasternack et al., 2021). While such literature has developed novel methodological approaches and advanced geomorphology, the financial expense and labor involved in these projects has limited the vast majority of meter-scale DEM analyses to only one or a few river reaches. As a result, there is a paucity of meta-analysis or sufficiently automated procedures to analyze and compare a large sample of river reaches at one time to draw statistically significant, generalizable geomorphic conclusions.

The question remains: how does a single hydro-morphodynamic process vary among river types? This study evaluated the role of a single hydro-morphodynamic mechanism – flow convergence routing (MacWilliams et al., 2006; Jackson et al., 2015) – in the five ephemeral river types found in California's South Coast region (Figure 1) to begin to answer this fundamental fluvial geomorphic question at the regional scale. As of yet, it is infeasible to attempt a continental or global scale analysis due to the lack of data, whereas there exists extensive high-resolution topo-bathymetric data of ephemeral rivers. The approach involved analyzing and comparing meter-scale fluvial DEMs to reveal and characterize similarities and differences in topographic patterning explained by flow convergence routing's relative importance as a channel altering mechanism in this setting.

This study advances geomorphic analysis methods and understanding through development of a new algorithm that (i) automates 1-m DEM generation from raw airborne lidar with more detailed attention to sources of uncertainty in river corridors compared to typical workflows used in the lidar industry, and (ii) implements the procedures from geomorphic covariance structure theory (Brown & Pasternack, 2014, 2017; Pasternack et al., 2018a,b; Pasternack et al., 2021) to evaluate hierarchical nesting of fluvial landforms within a river corridor and assess the hydro-morphodynamic mechanism of flow convergence routing. This new open-source code is freely available on GitHub (available at https://github.com/xaviernogueira/gcs_gui) and is thoroughly documented on "Read the Docs" (https://gcs-gui-documentation.readthedocs.io/).

1.1 Ephemeral rivers

Flashy ephemeral rivers have a hydrology characterized by short, high-intensity rainfall events that drive the largest annual discharges but otherwise have little to no flow between such events (Bull et al., 2000; Priddy & Clark, 2020). Similarly, intermittent rivers are seasonally ephemeral, with groundwater contributing to baseflow during the wet season. Together, ephemeral and intermittent rivers drain over half the world's land surface and are most common in arid, semiarid, and Mediterranean regions (Datry et al., 2017). For simplicity, we conceptually group intermittent and flashy-ephemeral stream hydrology and henceforth refer to both as "ephemeral".

Ephemeral river reaches have precipitation thresholds for channel flow, as opposed to precipitation contributing to a perennial baseflow. The thresholds vary with sediment

size, bedrock geology, river type, valley confinement, and vegetation (Hooke, 2016). The spatial heterogeneity of these variables often results in ephemeral rivers having more diverse annual flow regimes than perennial rivers within a given climatic setting (Hooke, 2016; Merritt et al., 2021).

Summarizing ephemeral river geomorphology is difficult; their fluvial processes and morphologies are diverse, spanning a wide variety of environmental settings globally. While many ephemeral river processes and channel forms are analogous to perennial rivers, others are quite distinct (Jaeger et al., 2017). Climate is one variable affecting channel morphology; in arid environments, with lower clay content and less-dense riparian vegetation, loosely consolidated channel banks promote wide split-channel/braided morphologies (Powell, 2009). Further, infiltration and evaporative transmission losses in ephemeral rivers can decrease sediment carrying capacity more than downstream slope reductions alone, therefore factors such as substrate infiltration rates and evaporative potential post-precipitation event can significantly contribute to network scale depositional patterns (Jaeger et al., 2017; Billi et al., 2018). Network transmission losses within ephemeral streams inhibit downstream transport of fine-grained sediments relative to that typical in perennial systems, contributing to poorly sorted channel sediments. In addition, low flood frequency in ephemeral rivers enables high rates of vegetation encroachment into the channel. Therefore, precipitation event recurrence partly controls channel hydraulic roughness, which in turn affects scour/deposition patterns (Segura-Beltran & Sanchis-Iborb, 2013; Hooke, 2016).

Like perennial rivers, ephemeral rivers organize in a network of diverse river types. In

the dry-summer subtropical climate, longitudinal position within an ephemeral stream network is the primary factor controlling channel morphology. As described by Jaeger et al. (2017), distinct morphologies are seen in the production, transfer, and deposition zones of an ephemeral stream network. The production zone, describing upland areas dominated by hillslope erosion, tend to have ephemeral river morphologies characterized by small, steep, single-thread channels with poorly sorted sediments and low width-depth ratios (Wohl & Pearthree, 1991; Jaeger et al., 2017). Upland channel morphology can appear quasi-stable between stochastic and quasi-periodic disturbances, such as El Niño/La Niña-driven wildfires and floods during anomalously strong years. Rare disturbances, especially when arriving in a fire-flood sequence, dominate sediment flux and channel evolution (Warrick et al., 2012; Gray et al., 2015).

Ephemeral rivers are ideal for automated geomorphic investigation because airborne LiDAR flown during the dry season provides complete river-corridor and channel-bottom coverage. Fluvial bathymetric LiDAR data availability is limited due to turbidity, depth, forest cover, and other constraints (Lague & Feldmann, 2020), and this has previously prevented comparative analysis among many river corridors in a single study. Focusing on ephemeral rivers affords such unprecedented spatial scale of analysis. However, one limitation is that study findings must be interpreted within the context of established and emerging geomorphological differences between ephemeral and perennial rivers.

1.2 Flow convergence routing

The topography of a river corridor is largely controlled by hydro-morphodynamic

processes driven by temporally variable discharge and sediment supply interacting with spatially heterogeneous fluvial topography (De Almeida & Rodriguez, 2012). The nature of this interaction can vary but has been studied as an assemblage of geomorphic processes that are linked to observed patterns of scouring and deposition (Wyrick & Pasternack, 2016). One such morphodynamic mechanism is ‘flow convergence routing’, which is broadly characterized by significant longitudinal topographic heterogeneity, inundated to various degrees depending on discharge, driving stage-dependent, non-uniform patterns of lateral and vertical flow funneling (i.e., convergence and divergence) resulting in longitudinal patterning of deposition and scour.

According to flow convergence routing theory (MacWilliams et al., 2006; Jackson et al., 2015), all else equal, a small cross-sectional area (i.e., geometric constriction) has a higher potential to scour and route sediment through it because flow streamlines come together thereby increasing velocity. Vice-versa, a large cross-sectional area causes momentum dispersion via streamline divergence, decreasing velocity and thereby increasing deposition. Further, the locations of small and large cross-sectional areas shift along the river corridor with water stage, because complex non-uniform river topography operates over different discharge ranges (Brown et al., 2015; Pasternack et al., 2018a, b). The velocity at any expansion or constriction may or may not become low or high enough, respectively, at a specific discharge to affect sediment deposition or scour, respectively. For low discharge, there could be intense but highly localized scour at a highly constricted “nozzle”, but insufficient sediment transport capacity to route that material further downstream. As a result, this relationship between cross-sectional

geometry and fluvial hydro-morphodynamics is expected to only control systemic landform patterning at the range of morphologically relevant discharges not only capable of mobilizing bedload but really transforming the terrain (Caamaño et al., 2009; Pasternack et al., 2018b; Pasternack et al., 2021).

Recent studies of a few river segments have now shown that there exists a threshold water stage above which landform structure is organized to be freely self-maintaining predominantly (but not exclusively) via flow convergence routing morphodynamics. For wide gravel/cobble lowland rivers and confined, steep mountain rivers, the threshold is identifiable in landform metrics for the cross-sectional area inundated by a discharge or stage one to two times that of bankfull. However, the channel-forming flow causing that change appears to be significantly greater (Pasternack et al., 2018b, 2021). In other words, a flow just inundating the bankfull channel identifies bankfull landforms but appears to have insufficient shear stress to wholesale change them. Meanwhile, a large flood inundating the width of a river corridor could really force bankfull landforms to conform to imposed hydraulics, while any peripheral floodplain, terraces, and other features might not subject to enough shear stress for them to change. To help convey these concepts we provide a flow chart that outlines the geomorphic implications of the different Ws, Zs covariance relationships possible at any given water stage (Figure 2).

1.3 Geomorphic covariance structure (GCS) and landforms

One key attribute of flow convergence routing theory is its ability to conceptually link a hydro-morphodynamic mechanism to quantifiable fluvial topographic patterning,

allowing its dominance as a fluvial process at a given discharge to be directly investigated from inundated topography alone. This contrasts most other fluvial hydro-morphodynamic analyses, as they typically use computed bed shear stress as an intermediary to explain topographic patterning. Some approaches to computing bed shear stress have unacceptable assumptions considering natural river nonuniformity, while others involve time consuming, financially costly, computationally intensive numerical modeling; all approach still yield estimates with high uncertainty.

The key to unlocking this morphology-process connection is the recent theory of geomorphic covariance structure (GCS) analysis first described by Brown and Pasternack (2014) and Brown et al. (2014). Subsequently, studies further articulated concepts, methods, and results, as summarized in the following brief overview of key GCS ideas. Detailed concepts and methods are left for readers to seek out especially in Pasternack et al. (2018a, 2021). There is also an online, free introductory GCS video presentation series beginning with https://youtu.be/VSMK72FbTfI.

There are many fluvial variables that can be quantified as they vary longitudinally downstream. A GCS is simply the linked bivariate pattern of any two of them. A GCS is not the statistic, covariance (a single number); it is the complete bivariate spatial series. The bivariate linkage of any GCS can be made using a decision tree or a mathematical operator such as the product- whatever helps reveal hydro-geomorphic processes. The GCS between a river's standardized width (Ws) and standardized, detrended bed elevation (Zs) (an inverse proxy for depth) has been shown to accurately predict the hydrodynamic mechanism involved in flow convergence routing (Pasternack et al.,

2018b).

Specifically, when Ws and Zs are both either positive or negative numbers at discharges capable of sediment routing, then flow convergent routing will maintain riffle-pool sequencing in an alluvial river. This is captured by the covariance product of Ws and Zs, C(Ws, Zs), which is calculated across the complete bivariate spatial series. Flow convergence routing theory anticipates that Ws and Zs series positively covary (i.e., $C(Ws, Zs) > 0$) at morphodynamically relevant water stages (Pasternack et al., 2018). Vice versa, channel dimensions with negative Ws and Zs covariance (i.e., $C(Ws, Zs) < 0$) are thought to be asynchronous with flow convergence routing driven hydrodynamics and unstable in rivers at channel-altering discharges, unless the bed is highly resistant to hydraulic forcing.

Because of its ability to discern between these two topographic regimes, the GCS of Ws and Zs has previously been utilized to predict at which stage fluvial hydraulics switch from minimally channel altering to having appreciable, channel altering flow convergence routing morphodynamics (Brown & Pasternack, 2017). GCS analysis of a river's DEM can be used to study flow convergence routing via quantification of Ws and Zs over a range of discharges. Because GCS analysis requires only a DEM as an input (Pasternack et al., 2021), without numerical modeling or reliance on discharge-stage gage data, it is possible to study remote fluvial topographies that are less impacted by human alterations (Wohl, 2019). Incidentally, the same GCS has been found to be an important control on river hyporheic exchange rates (Movahedi et al., 2021), so the methodology is relevant beyond just morphodynamics.

Pasternack et al. (2021) recently reported that confined mountain rivers with coarse bed material and exposed bedrock have a threshold stage at which the GCS between Ws and Zs changes from negative to positive. This provides a simple test to determine what discharge it takes to not merely move bed sediment but organize fluvial landforms- a more important fluvial function. What remains unknown is the extent to which cross-sections with positive Ws and Zs values occur at different water stages across diverse river types, and whether they have riffles/pools, other riverbed units (e.g., cascades, steps, alternate bars, lateral benches, etc.), or no units at all (i.e., a straight, flat uniform canal).

1.4 Study goals

While the findings of previous flow convergence routing studies have direct relevance to river restoration design and environmental flow management contexts, especially where maintaining resilient channel bed undulations is frequently prioritized (i.e., riffle-pool sequences), it remains uncertain due to small sample sizes whether flow convergence routing is similarly present across diverse river types. The purpose of this study is to address this uncertainty by analyzing the GCS of standardized width (Ws) and standardized, detrended bed elevation (Zs) that characterize flow convergence routing in ephemeral rivers, and do so at three key water stages that address different magnitude events. The three key water stages are baseflow, bankfull flow, and a flood flow at a geomorphically significant stage (section 2.6).

We statistically investigated whether flow convergence routing’s dominance or its

relationship with water stage is significantly different across river types. For example, a central scientific hypothesis evaluated states that river types characterized by channel bed undulations (i.e., riffle-pools, or step-pools) will have GCSs at bankfull that match the expectations of flow convergence routing theory, suggesting that flow convergence routing is central to the maintenance of said undulations. Additionally, we hypothesize that the water stage at which flow convergence routing is most dominant will change for different river types, potentially as a function of confining valley wall distance or sediment size. For instance, because coarser sediment is mobilized at higher flow velocities, we expect that upland rivers will have an onset of positive C(Ws, Zs) channel topography at a higher water stage than for lowland river types with finer bed material. We also hypothesize that because expansive floodplains disperse the energy of the highest water stages, flow convergence routing morphodynamics in unconfined valleys will peak at intermediate water stages constrained by channelized topography (i.e., highest C(Ws, Zs) at bankfull stage).

To test these hypotheses and chieve study goals regarding ephemeral rivers, we formed two objectives, each with specific, tractable questions. Objective 1 (O1) is to assess the degree to which active channel morphology at three key water stages is consistent with flow convergence routing acting as a dominant hydro-morphodynamic mechanism. Our second objective (O2) is to investigate the extent to which South Coast ephemeral river channel bed elevation undulations (O2a) and landforms (O2b) are a product of hydro-morphodynamics driven by larger scales of topography (i.e., valley wall topography affecting flood flows hydraulics). We addressed Objective 1 by answering

three questions (O1a,b,c) that explore differences between river type and water stage longitudinal topographic deviations as expressed by Ws and Zs series. Such differences are interpreted in relation to the particular pattern of topographic nonuniformity required by flow convergence routing (i.e., positive C(Ws, Zs)).

Objective 2 aimed to move beyond typical fluvial research where the landforms and morphodynamics of a given channel dimension are understood by considering drivers for that same dimension. For example, studies of the bankfull channel focus on hydro-morphodynamics in the bankfull channel. Yet in nature a wide, deep ‘pool’ section of the bankfull channel could be a product of a valley wall bedrock outcrop that constricts flood flows, increasing flow velocity, and therefore inducing local scour. Objective 2 investigated such multi-scale drivers of fluvial topography, which contributes to our overall study goals, because as described by flow convergence routing theory (section 1.2), it may take stronger forces than can be produced within a given channel dimension to change and control it. Therefore, resilient low flow channel dimensions may be maintained by patterns of topographic nonuniformity at higher water stages capable of making channel alterations. Theoretically, a similar relationship between bankfull and flood-stage channel dimensions could also exist but has been less studied. In South Coast ephemeral rivers with their characteristic sporadic but intense flood flows, it’s possible that these discharges are the dominant driver of lower water stage channel morphology. On the other hand, many bankfull flows are likely to be morphologically relevant themselves and could potentially rework, and obscure, the channel alterations left by flood flows. A flow chart outlines both objectives, their associated questions, and

hypotheses (Figure 3).

1.5 Scientific questions and hypotheses

1.5.1 **Question O1a:** To what extent does longitudinal Ws and Zs covariance change with water stage, and does this vary among ephemeral river types?

Here we investigate how C(Ws, Zs) may change with water stage among different South Coast ephemeral river types. High C(Ws, Zs) at a given water stage suggests that flow convergence routing is playing a dominant hydro-morphodynamic role (section 1.3). Using this framework, we make several hypotheses. First, we hypothesize that for all river types C(Ws, Zs) will be lowest at baseflow, which in many cases would lack the ability to significantly alter channel morphology. Building on this logic, we also hypothesize that average C(Ws, Zs) will increase with water stage for all river types except any river type characterized by expansive floodplains that would disperse overbank flows, significantly dissipating flow velocity, and therefore disrupting the hypothesized relationship between water stage hydro-morphodynamic relevance. Finally, we hypothesize that the high width to depth ratio of partly confined braided rivers will weaken width-driven flow convergence routing and result in the lowest average C(Ws, Zs) values of all river types.

1.5.2 **Question O1b:** Do stage-dependent bivariate distributions of cross-sectional Ws and Zs values aggregated among a river type display non-Gaussian organization, and does this vary by water stage or river type?

In contrast with the previous question in which river reach averaged C(Ws, Zs) values were compared, to answer question O1b we qualitatively assessed the entire bivariate distribution of paired cross-sectional Ws, Zs values for each river type among the three key water stages. Exploring joint Ws, Zs distributions allows changes in the relationship between Ws and Zs with water stage or river type to be qualitatively described visually and interpreted beyond what single-value metrics facilitate.

Because Ws and Zs are both standardized values, if width (W) and relative bed elevation (Z) have no structured relationship (i.e., random or uniform bivariate distribution), the Ws, Zs bivariate distribution would appear symmetrically Gaussian. We assessed each 2-D distribution qualitatively by describing the degree of clustering, and the nature of any prominent non-Gaussian skew or linearity. Diagonal linearity would suggest a non-negligible level of Ws, Zs covariance with either a positive or negative sign. For example, if the average C(Ws, Zs) is very high for a river type at some flow, the bivariate distribution will have a positive sloping diagonal linearity, and vice versa.

We hypothesize that South Coast ephemeral rivers in confined mountain canyons will have more tightly clustered bivariate Ws, Zs distributions due to valley proximity restricting the range of possible topographic variability. Additionally, we hypothesize that unconfined rivers with uniform sand bedded channels at flood stage and partly confined

braided rivers across all water stages, for which in the previous question we hypothesized low average C(Ws, Zs), will have bivariate Ws, Zs distributions that appear Gaussian.

1.5.3 **Question O1c:** How do the relative abundances of flow convergence routing landforms vary across flow-stages and ephemeral river types?

While question O1a uses river averaged C(Ws, Zs) values, it can also be illuminating to focus specifically on the subset of high-variability cross-sections that have both Ws and Zs more than 0.5 standard deviations from their reach mean values. We use the sign of Ws and Zs to classify such cross-sections as one of four named flow convergence routing landforms differentiated from a “normal channel”: oversized (Ws+, Zs-), constricted pool (Ws-, Zs-), nozzle (Ws-, Zs+), or wide bar (Ws+, Zs+). These landform names describing individual cross-sections were created in recent research to help establish a conceptual linkage between bivariate channel dimensions and commonly delineated fluvial morphology features (Pasternack et al., 2018a). Nozzles and oversized landforms are associated with negative C(Ws, Zs) values, and are predicted to be morphologically unstable during channel altering flows by flow convergence routing theory – unless bed and banks are highly resistant to erosion. Vice versa, the wide bar and constricted pool landforms have positive C(Ws, Zs) values and are hypothesized to be freely maintained by flow convergence routing dominant hydro-morphodynamics (section 1.3). Because the non-normal landforms are defined using the same 0.5 standard deviation threshold, in lieu of a relationship between Ws and Zs,

we would expect to see equal abundances of the different non-normal landforms.

We hypothesize that nozzle and oversized landforms will be most prevalent at baseflow in all river types. We make this prediction because baseflows are typically non-channel altering and both negative C(Ws, Zs) landforms are non-resilient during flow convergence routing driven channel alterations. Therefore, nozzles and oversized landforms would be most likely to survive within the baseflow channel. Additionally, we hypothesize that nozzles and oversized landforms will be more common at higher water stages (i.e., bankfull and flood stage, section 2.6) in confined, cobble-boulder, cascade/step-pool rivers, because such very coarse sediment and high-relief bedforms require much higher bed shear stress to mobilize, let alone fully alter the channel, and that necessitates a higher water stage. Finally, we hypothesize that partly confined riffle-pool river reaches will have a greater abundance of constricted pool and wide bar landforms at bankfull, which would be consistent with their presumed channel morphology.

1.5.4 **Question O2a:** Are relative topographic highs and lows at baseflow and bankfull stages associated with width undulations occurring at bankfull and flood stage topography, respectively?

For Objective 2 we study how Ws and Zs shift as water stage increases with the aim of assessing the degree to which higher water stage hydro-morphodynamics controls lower water stage channel morphology. Question O2a contributes to this objective by statistically investigating the possibility that baseflow Zs undulations are a product of

bankfull Ws-driven hydro-morphodynamics, as well as the analogous relationship between bankfull and a higher flood stage. For example, the shallow, high Zs cross-sections of some rivers at bankfull may be wider on average during a flood stage than the deep, low Zs bankfull cross-sections. This would suggest that the flood stage's channel dimensions are at least somewhat responsible for bankfull channel Zs patterns. Finding the inverse relationship, or no relationship at all, between a lower and higher water stage would challenge the notion that flow convergence routing during higher flows is a relevant driver of lower flow channel dimensions.

We hypothesize that all river types will have high Zs cross-sections nested within wider than average portions of channel at the next higher water stage, and vice versa. Additionally, we hypothesize the resilient Zs undulations found in partly to fully confined riffle-pool and step-pool river types 3 will be maintained by the strongest wet season flood flows. Therefore, we predict that only their bankfull channel Zs undulations will significantly positively covary with flood stage Ws.

1.5.5 **Question O2b.** Do flow convergence routing landforms have preferred nesting structures (e.g., baseflow nozzles within bankfull wide bars)?

Using classic terminology, the previous question is about landform "nesting" – the presence of forms within forms – but considers individual variables rather than whole landforms. We continue to investigate potential hydro-morphodynamic relationships between water stages by looking for preferential nesting patterns amongst the subsect of cross-sections with non-normal landform designations (section 1.5.3). Flow

convergence routing, building on classic velocity reversal theory, anticipates preferred landform nesting structures between the active channel topography of a low flow (i.e., baseflow) and bed load mobilizing bankfull discharge (Pasternack et al., 2018a,b). For example, a wide bar or nozzle (+Zs) at baseflow is expected to be nested within a depositional wide bar at bankfull, maintained by width expansion forced flow divergences that reduces sediment carrying capacity (section 1.2).

To answer question O2b, we statistically characterized the nature of channel landform nesting structures across both water stage transitions for all ephemeral river types. We hypothesize that nozzle and oversized landforms at baseflow will be preferentially nested within wide bars and constricted pool at bankfull, regardless of river type. We make this prediction because negative covariance landforms composed of non-cohesive sediment are theoretically non-resilient at water stages with channel-altering bed shear stress. Baseflows are typically insufficient to yield bed shear stresses that can alter landforms, therefore the difference between bed shear stress patterns at baseflow versus higher discharges potentially facilitates a prominent landform covariance “reversal”.

Additionally, we hypothesize that such preferential nesting of negative covariance landforms within positive ones will be subdued going from bankfull to flood stage for unconfined sand-gravel, partly confined braided, and confined plane bed river types. For partly to fully confined riffle-pool and step-pool river types, we suggest that flood stage flow convergence routing may be responsible for maintaining their characteristic channel Zs undulations.

1.6 Study area: South Coast climate and geomorphology

California's 'South Coast' region (Figure 1) is a regulatory area defined by the California Water Board (Byrne et al., 2020a) along the state's southern Pacific coastline. The region consists of coastal valleys, foothills, and rugged coastal mountain ranges that loosely share physiographic characteristics despite significant geologic diversity. The South Coast region has a largely dry summer subtropical climate with seasonal precipitation bipolarity (Inman & Jenkins, 1999., Abatzoglou et al., 2009). There is typically little to no precipitation during the May to October dry season followed by a considerable amount of atmospheric river-driven precipitation during the November to April wet season (Dettinger et al., 2011; Polade et al., 2017), though even then rainfall is intermittent. South Coast precipitation is also spatially heterogenous, made evident by the 30-year mean February precipitation, historically the wettest month of the year, ranging from 8 cm to 30.5 cm (Hill et al., 2016) within the region.

Coastal U.S. rivers are generally sediment rich (Pfieffer et al., 2016), and the South Coast region is no exception. Active and complex faulted geology in the mountain regions, an abundance of unconsolidated Cenozoic sediments, as well as erodible sedimentary lithologies all contribute to high rates of hillslope denudation during wet season precipitation events (Inman & Jenkins, 1999). Inter-annual ENSO-driven climatic variability can also contribute to hillslope denudation; strong El Niño years, which reoccur roughly every five years, have resulted in 27x increases in South Coast stream sediment fluxes (Inman & Jenkins, 1999; Abatzoglou et al., 2009). In addition, the region's wildfire regime alters soil conditions (Wohlgemuth et al., 1999) and increases

hillslope smoothness (Roth et al., 2020). When wildfires are followed by intense wet season rainstorms, then mass wasting loads rivers with large quantities of sediment (Warrick et al., 2012).

2 Methodology

2.1 GCS analysis Python program

Until now, GCS analysis has been performed manually using GIS and Excel (Pasternack et al., 2018b, 2021), which limits the number of reaches that can be analyzed and raises the potential for manual error at many steps. This study introduces an open source Python3 program that reproduces the existing GCS workflow (Figure 4) while adding several new outputs and analyses.

The program requires a topo-bathymetric LiDAR point cloud LAS file as the primary input. Expert-based user input then specifies three things: (i) LiDAR processing parameter values used in LasTools, (ii) thalweg elevation profile breakpoints in support of bed-elevation detrending (section 2.5) and (ii) a set of key water stage values above Zd (hereafter, Zd stages) that are representative of geomorphically, hydrologically, or ecologically significant inundation levels (section 2.6). The program requires LasTools (Hug et al., 2004), ArcPro's (ESRI, 2011) Python3 package 'arcpy' (with a valid 'spatial analyst' license), and a few free Python packages (i.e., pillow, plotly, seaborn, and openpyx1).

As the main feature, the program automates production of downstream spatial series of

Ws, Zs, C(Ws, Zs), and flow convergence routing landform code values for all selected key Zd stages. It also produces a set of reach-average river metrics by Zd stage that can be used for river classification. From the primary GCS spatial series, the program then carries out several analyses to evaluate GCS patterns and flow convergence routing conditions. Analyses include data tables of indicator metrics and plots of results. All details are in the manual at https://gcs-gui-documentation.readthedocs.io/.

2.2 Experimental design

Given the new GCS program, a mindful experimental design was needed to answer the study questions by analyzing GCS outputs to compare and contrast results among many reaches representing the diversity of South Coast river types. The overall scientific method began with a river-reach sampling scheme (see section 2.3). Even though GCS analysis is now reasonably automated, in this first implementation we did not aim to extract and analyze the entire river network, as some mindful manual decisions must be made for every reach. The initial expectation of river type came from a pre-existing reach type prediction vector file made with a machine-learning algorithm applied to desktop GIS metrics (Guillon et al., 2020).

Once selected, individual reaches were put through the GCS program to obtain standard GCS analysis outputs and reach-average river classification metrics based on the high-resolution LiDAR data. Next, program outputs were used to verify and possibly update river types (see section 2.8). Finally, Python scripted analyses were used to produce statistics, plots, and tables that addressed the scientific questions (section 1.5).

2.3 River type sampling

According to Byrne et al. (2020a), a river type is defined as an archetypical stream form at the 10 – 20 channel width scale (e.g. riffle-pool, plane bed, etc.) that has: (a) well-defined channel attributes (e.g. slope, bankfull width, etc.), (b) topographic variability attributes (TVA) (e.g. coefficients of variation of width and depth), (c) sediment composition (e.g. D50, D84, etc.) and (d) landscape location (e.g. valley confined, partly confined or unconfined) that can be verified in the field. A data-driven, bottom-up, statewide river classification was previously developed for California using > 1,100 sample sites, along with eight more-detailed, more-accurate regional classifications (Lane et al., 2021). The classification methodology was first piloted for the ~ 70,000 km^2 Sacramento River catchment (Lane et al., 2017), which revealed that channel types were largely independent of catchment hydrology (Byrne et al., 2020b).

Byrne et al. (2020a) added five regional classifications, including for the South Coast region. South Coast reach sampling was designed using a rigorous, equal-effort, three-way (valley confinement, sediment supply, and local slope versus contribution area bin) stratified random sampling strategy. The field campaign was carried out by trained professionals from the Southern California Coastal Water Research Project. Field data were processed into a multivariate statistical classification with maximally contrasted but representative river types using a standardized procedure codified in R Markdown. Statistical analyses that aided classification and understanding/interpreting classification results included non-metric multidimensional scaling (Anderson, 2001), Ward's clustering algorithm (Ward, 1963), and classification and regression tree analysis

(De'ath & Fabricius, 2000).

Qualitative descriptions of each river type are displayed (see Table 1), along with plots visualizing the distribution of classification relevant river metrics (Figure 5). South Coast river types exist in three valley confinement settings: unconfined (river type 1), partly confined (river type 2, river type 5), and confined (river type 3, river type 4). River types 3 and 4 capture production zone ephemeral morphologies. River types 1, 2, and 5 capture the morphological diversity within the transfer zone of an ephemeral stream network, where floodplains are present and sediment balances are often characterized by quasi-equilibriums or long-term net deposition (Jaeger et al., 2017).

Hand in hand with the classification based on a modest number of observable sites, Guillon et al. (2020) developed a machine learning algorithm that predicts river type for any 200-m river interval along National Hydrography Dataset version 2 stream lines (McKay et al., 2012; NHDPlusV2) on the basis of desktop GIS metrics. The algorithm was trained using the field-observed river type labels. Byrne et al. (2020a) further expanded the machine learning algorithm and applied it to all coastal regions, including the South Coast region. This yielded a population of reaches with expected river types to draw from for use in a mindful sampling campaign in our experimental design.

To reduce possible bias and avoid noticeable geographic patterning in the analysis related to river reach sample quantities, we assembled relatively even-sized numbers of each river type. The population of 200-m river intervals from Byrne et al. (2020a) was clipped to be within the area of available, suitable dry-season LiDAR data producing full

river-corridor topography (i.e. no standing water that near-infrared airborne LiDAR could not penetrate). Among those intervals, the population was further reduced to isolate reaches with ephemeral hydrology, as identified by a statewide hydrologic classification's "Flashy-Ephemeral River (FER)" designation (Lane et al., 2018).

From the population of all ephemeral reaches with LiDAR coverage and machine-learning predicted river types, eight were randomly sampled for each river type. These forty sites served as a representative initial sample set to undertake further characterization to determine final suitability for use in the study. The sites were not yet considered final, because the study's analysis of dense LiDAR point clouds yielded classification metrics that could check the machine learning prediction and possibly override it (section 2.8) for a more accurate classification beneficial for this study.

2.4 DEM generation and river study length selection

Meter-resolution, bare ground raster DEMs were generated for an extra-long and wide segment of fully dry river-corridor terrain using the steps outlined in Figure 4a. Only LiDAR data meeting the U.S. Geological Survey's rigorous 3D Elevation Program standards were used (Table 2). Data had a 0.7-m maximum mean point spacing and a 10-cm maximum vertical accuracy root mean squared error (RMSE). Normalized Differenced Vegetation Index meter-resolution rasters were generated from National Agriculture Imagery Program four-band imagery to apply different LasTools parameters on vegetated and non-vegetated areas. The resulting point clouds with bare-ground elevation values were converted to 1-m resolution raster DEMs. [A flow chart detailing

our LiDAR processing methodology is in Appendix 1.] DEMs were closely examined for quality issues; river reaches with water-filled pools or artificial human confinements (levees, walls, etc.) were removed from the sample set reducing the original 40 reaches down to 35. [A table listing all sampled river reaches is in Appendix 2.]

Next, each DEM's length was clipped to assure that samples represent a persistent geomorphic reach of a single river type. We identified river type transitions manually with visual DEM interpretation, aided by aerial imagery. Significant changes to bankfull channel or valley slope, width, planform pattern, large bed elements, and bed material served as indicators of a change in river type. Site lengths varied between 410 and 2207 m, averaging 1057 m (± 453 m). The average is 56 times mean channel width at bankfull, indicating that the study involved substantially long reaches suitable for GCS analysis consistent with classic reach length norms for quantification procedures.

2.5 DEM detrending

GCS analysis focuses on local fluvial topographic variability as a hydro-morphodynamic driver via topographic steering, necessitating DEM detrending using the steps in Figure 4b. The first sequence of steps creates and analyzes a thalweg pathway. Bare-ground DEMs were smoothed via a low pass filter (15 passes) before a thalweg polyline was generated using a least-costs algorithm applied to the smoothed DEM. Elevation values from the unsmoothed bare-ground DEM were extracted in 3 ft (0.91 m) increments along the thalweg and plotted. Major slope breaks were visually identified and used to apply a piecewise linear regression to the longitudinal thalweg elevation series.

We next generated a detrended DEM by subtracting the regression modeled elevation value for each sampled thalweg point from all raster cells nearest to that thalweg point (Figure 6). The quality of a detrended DEM declines with distance from the thalweg, and in arid rivers can be negatively affected by in-channel shrubs (Segura-Beltran & Sanchis-Iborb, 2013, Hooke, 2016). Shrubs are especially difficult to penetrate using LasTools point cloud processing algorithms (Norheim et al., 2002; Gould et al., 2013). Imagery showing the detrended DEM of each sampled river is provided in Appendix 3

2.6 Baseflow, bankfull, and flood Zd stage designation

To compare fluvial topography among river reaches and river types we defined Zd stages (i.e., horizontal water surface elevations above the detrended bed elevation, Zd) that seemed geomorphically similar among all sites, even though sampled rivers came in different shapes and sizes. For a standardized detrended DEM, water stage is identified with a Zd value, thus it is referred to as a Zd stage (Pasternack et al., 2021). For each sampled river, a Zd stage is designated that corresponds to a longitudinally persistent, eco-geomorphically relevant stage threshold; at a minimum, stages corresponding to ‘base flow’ and ‘bankfull’ discharges are used (Figure 7). Unless the floodplain is exceptionally flat and wide, one or more flood stages should be included, such as each stage associated with different macro-channel bench tops (Erskine & Livingstone, 1999), the stage inundating the flood prone area (Pasternack et al., 2021), and/or the stage filling the alluvial valley floor. The more Zd stages analyzed, the more complex the analysis and interpretation of how all the stages work together, which

remains an open challenge for future GCS development.

Zd stage selection is an expert-based process facilitated by an analysis of lateral slope breaks across a river corridor's width and inspection of aerial imagery (Figures 4c and 7). The procedure for selecting Zd stages involves generating wetted area polygons at 3-cm (0.1-ft) Zd increments by differencing the DEM from each Zd stage plane. The wetted areas of these polygons are plotted as a function of Zd. In the plot, a high area-vs-Zd slope indicates that the riverbank has a gentle lateral slope (i.e., a small increase in stage inundates more bank terrain) and a low area-vs-Zd slope indicates steep riverbanks. Hence, slope breaks identify Zd stages of transitions between channelized and flat terrain. Aerial imagery, the detrended DEM, and field observations/experience were used to identify and select the slope break that represent eco-geomorphically significant conditions, such as baseflow stage, bankfull stage, and the stage that fills the flood prone area (Pasternack et al., 2021).

The South Coast's ephemeral rivers do not have perennial, groundwater-derived 'base flow' (Dettinger et al., 2011; Polade et al., 2017), but they do tend to have a flat channel bottom, sometimes containing many large bed elements. For this study, baseflow Zd stage was defined as that just fully inundating the relatively flat riverbed along the majority of the thalweg's longitudinal extent. DEM detrending results in high riffle crests protruding above the baseflow Zd stage because topographic analysis cannot account for hydraulic backwatering (Pasternack et al., 2021). In partly confined and unconfined valleys, bankfull Zd stage was defined as that inundating a geometrically well-defined channel bounded by a comparatively flat depositional surface (i.e., floodplain). In

confined canyons without floodplains, bankfull Zd stage was delineated to exclude densely vegetated peripheral areas lacking non-boulder, active, alluvial bed sediment. In partly confined valleys, flood Zd stage was defined as the lowest stage inundating the alluvial valley and contacting confining valley walls. In some unconfined settings with especially distal valley walls, a flood Zd stage may be defined regarding a prominent terrace feature that limits the wetted areas corresponding to all realistic water stages. Flood Zd stage can be defined similarly in some confined settings as well, in which a small but observable alluvial valley is present. In the most tightly confined reaches without any semblance of a floodplain, flood Zd stage is defined by both the slope break above which wetted area accumulation increases linearly with Zd stage and careful visual interpretation of paleo-flow indicators.

2.7 GCS data extraction

GCS analysis requires Ws and Zs data from evenly spaced cross-sections along the river corridor. Unless a canyon is highly confined (e.g., Pasternack et al., 2021), a river's flow path usually changes with discharge (Pasternack et al., 2018a). Changes are most notable when Zd stage thresholds are exceeded, and momentum significantly straightens and shortens the flow path. The method to address this involves generating a centerline bisecting the wetted area for each Zd stage.

Next, cross-sectional rectangles were generated and stationed at ~ 1/20th of bankfull width (but larger than the dimensions of a single raster pixel). To compare data at rectangles along centerlines of different lengths, data from higher Zd stages were

spatially joined to the nearest base flow cross-section rectangle. Densely spaced, adjacent base flow stations may share the same bankfull or flood Zd stage; so no interpolation was performed. [Cross-section spacings for the 35 study reaches are provided in Appendix 2.]

Fluvial topography was processed to obtain longitudinal spatial series and GCS metrics. Mean wetted width (W) was calculated at each Zd stage by clipping cross-sectional rectangles to the wetted area polygon, quantifying the wetted area of each clipped rectangle, and dividing those values by each rectangle's downstream length. Mean detrended bed elevation (Zd) was calculated by using zonal statistics to extract the mean detrended DEM cell value below each wetted area clipped cross-sectional rectangle.

For both W and Zd, values were standardized to yield Ws and Zs. Reach-average values were first subtracted from individual rectangle values. Then the residual was divided by the reach standard deviation of values. For this study, geomorphic covariance, C(Ws, Zs), was calculated using the product (Ws·Zs) to obtain a spatial series at each key Zd stage (e.g., Figure 8).

Finally, we used a decision tree to classify each rectangle into one of five stage-independent, morphodynamics-specific landform types: 'normal channel', 'nozzle', 'wide-bar', 'constricted pool', or 'oversized' (Figure 9). Wide bar and constricted pool units have positive C(Ws, Zs) and are self-sustainable by flow convergence routing. Nozzle and oversized have negative C(Ws, Zs) and are expected to scour or fill,

respectively, if nozzles are alluvial and if there is a sediment supply to fill oversized (Pasternack et al., 2018b).

2.8 River type verification

The 35 study sites obtained through the sampling procedure had uncertainty as to their river type arising from two sources: statistical methods to create the regional classification from a modest number of samples and machine learning prediction of the South Coast river type of every 200-m stream interval (Byrne et al., 2020a). For this study to be scientifically meaningful, river type designation must be highly accurate, within the limitations of classification itself as a paradigm. Rather than move forward assuming the types were correct, the detailed detrended DEMs and aerial images available for this study enabled desktop-based quantitative and expert-based verification (and reassignment, if necessary) of each study site's river type.

Four reach-average attributes found in the South Coast river classification (Byrne et al., 2020a) that varied strongest with river type provided a quantitative basis for classification: slope, valley confinement distance, bankfull width to depth ratio, and bankfull depth coefficient of variation (Figure 5). The GCS program was used to compute these variables at bankfull Zd stage for each site's DEM. Resulting values were used in the classification and regression tree that orders variables into their relative place for keying South Coast river types at each site (Byrne et al., 2020a), with the exception that no grain size classification metrics were available.

After verification and some re-assignment, each river type had six to eight samples (Table 1). Sensitivity analysis was conducted to assess the extent to which channel-type sample sizes impacted class-averaged GCS metrics. All groups' sample size was found sufficient to prevent the exclusion or inclusion of any given river reach from significantly affecting class-averaged GCS values. [Detailed characterizations of each site and its final river type assignment are in Appendix X.]

2.9 Data analysis by question

2.9.1 **Question O1a:** To what extent does longitudinal Ws and Zs covariance change with water stage, and does this vary between river types?

Extracted longitudinal C(Ws, Zs) series were used to calculate mean C(Ws, Zs) and the percent of cross-sections with positive C(Ws, Zs) (hereafter "covariance metrics") for all reaches at the three key water stages. If channel width and bed elevation are independent, then the expectations for mean C(Ws, Zs) and % C(Ws, Zs) > 0 values are 0 and 50%, respectively. Results significantly above or below expectation indicate the Ws and Zs are co-varying to yield a coherent pattern per hypotheses.

To address question O1a, values for each metric were segregated by river type and water stage, and then a Welch's t- was applied. This tested whether the population of values of each metric for a given river type at any water stage had an equal mean to that of any other stage, within 95% confidence ($p < 0.05$) and used to quantify for each river type whether a metric changed significantly on average with water stage. Similarly,

we tested whether the mean values of each metric differed significantly between river types at a given Zd stage.

2.9.2 **Question O1b:** Do stage-dependent bivariate distributions of cross-sectional Ws and Zs values aggregated among a river type display non-Gaussian organization, and does this vary by water stage or river type?

All paired Ws and Zs cross-sectional values from our full sample of South Coast ephemeral rivers were segregated first by river type, and then by key Zd stage (5 types times 3 stages yielded 30 subsets). For each two-way stratified dataset, a density heat plot was produced that visualizes the distribution of all cross-sectional geometries as captured their standardized Ws and Zs values.

As previously described (see section 1.5.3), due to the nature of standardized values, a symmetrical, Gaussian-like joint distribution would affirm the null hypothesis that width and bed elevation have no structured relationship. Because thousands of cross-sections are visualized in each heat plot, any noticeable non-Gaussian-like skews or linearity are unlikely to emerge by chance. To address our hypotheses, we qualitatively compared and interpreted heat plots across the key water stages for each river type, as well as plots across different river types at the analogous Zd stages.

2.9.3 **Question O1c:** How do the relative abundances of flow convergence routing landforms vary across water stages and river types?

The relative abundance of cross-sections with each landform classification (see section

2.5) at baseflow, bankfull, and flood Zd stage was calculated for all sampled river reaches (i.e., % nozzle, % wide bar, etc.). Next, we consolidated these relative abundance values first by river type, and then sorted them by key Zd stage.

In lieu of a relationship between Ws and Zs for a river type at a given Zd stage, we would expect to see approximately uniform abundances of the different non-normal landforms, so this was tested first. The analysis of variance test (ANOVA) produces p values representing the probability that observed discrepancies between averaged landform relative abundances are statistically significant. Additionally, separate hypotheses predicted that certain landforms will be differently abundant across river types at the same Zd stage. We addressed these with a different ANOVA that compared the average abundance of each non-normal landform type across river types to a uniform distribution. Hypotheses were considered corroborated only if the observed landform abundances matched predictions and were significantly differ from a uniform distribution, as indicated by an ANOVA p value < 0.05.

2.9.4 **Question O2a:** Are relative topographic highs and lows at baseflow and bankfull stages associated with width undulations occurring at bankfull and flood stage topography, respectively?

For each river type, we identified the subsets of cross-sections with high Zs (> 0.5) and low Zs (< -0.5) at baseflow and bankfull Zd stages. We then extracted the Ws values of these cross-sections at the next higher Zd stage, either bankfull or flood. To address hypotheses, we paired and compared the distributions of the higher Zd stage Ws values

associated with high and low bed elevation. To do so we visualized each pair of Ws distributions in Violin plots and used a Welch's t-test (Yuen, 1974) to test whether population averages were significantly different at the 95% level ($p < 0.05$). For example, one hypothesis expects that regardless of river type, cross-sections with low baseflow Zs will have lower average Ws at bankfull Zd stage than cross-sections that have high baseflow Zs. This hypothesis would be confirmed if the predicted difference in means is observed and found to be statistically significant at the $p < 0.05$ level.

2.9.5 **Question O2b.** Do flow convergence routing landforms have preferred nesting structures (i.e., baseflow nozzles within bankfull wide bars)?

For both baseflow-in-bankfull and bankfull-in-flood landform nesting, we identified all cross-sections that changed from one non-normal flow convergence routing landform to another. To address hypotheses, we assessed for each river type whether any specific landform transitions were over or underrepresented relative to random change using Chi-Square tests (Lowry, 2017). The tests checked the significance of discrepancies between the expected and observed frequency of each unique landform transition. The Chi-Square test's 'expected frequency' parameter was set to the relative abundance landforms at the higher paired water stage. For example, if on average 15% of a river type's flood stage cross-sections are classified as wide bars, then the expected frequency for any bankfull landform transitioning to wide bar is 15%. This allows preferred nesting structures to be tested for significance relative to any changes in landform abundances between water stages. For instance, building on the previous

hypothetical, if much more than 15% of bankfull cross-sections with a given landform classification transition into wide bar, and the Chi-Squared test p value is < 0.05, then we could conclude that there is a preferential landform nesting pattern.

3 Results

3.1 **O1a.** Low and high covariance values for baseflow and bankfull stages, respectively

Results corroborated the hypothesis that both covariance metric values, mean C(Ws, Zs) and % C(Ws, Zs), would be lowest (more negative Ws, Zs covariance) for all river types at baseflow, and then increase with stage (Table 3). The results of the t-test comparing baseflow covariance metrics with both higher stages were at a statistically significant level for confined and partly confined river types 3, 4, and 5 ($p < 0.05$). In these three river types, cross-sections that are shallower tended to be narrower as well, and vice versa. Base flow hydraulics were therefore too weak to force the topography in these three river types to adjust to them.

Shifting from baseflow to bankfull stage, large, statistically significant increases in mean C(Ws, Zs) and % C(Ws, Zs) > 0 (more positive Ws, Zs covariance) were observed for river types 1, 3, 4, and 5 (Table 3). River types 3, 4, and 5 each had on average ~ 20% more positively covarying cross-sections at bankfull than at baseflow. At bankfull, all river types had on average > 50% of cross-sections with positive C(Ws, Zs) values. Additionally, all river types had mildly positive mean C(Ws, Zs) except for river type 3.

Finally, we compared bankfull and flood stage and found that both mean C(Ws, Zs) and % C(Ws, Zs) > 0 did not significantly differ between stages in river types 1, 2, 4, and 5. River type 3 experienced a statistically significant 0.30 increase in mean C(Ws, Zs) going from bankfull to flood stage, as well as a ~ 10% increase in positively covarying cross-sections on average ($p = 0.045$ and $p = 0.046$ respectively).

Results do not support either of our river-type-specific hypotheses. While river type 1 does have highest average covariance metric values at bankfull, they were not statistically significantly higher than flood stage as we predicted. Additionally, river type 2 did not have the lowest average covariance metric values of all river types at any water stage (see section 1.5.2 for the full prediction justification). [All question specific hypotheses are color coded in accordance with our study's findings in Figure 3]

3.2 **O1b.** Do stage-dependent joint distributions of cross-sectional Ws and Zs values display non-Gaussian organization, and does this vary by water stage or river type class?

River type 1 (unconfined, uniform, sand/gravel) joint Ws, Zs distributions have a roughly Gaussian form at both baseflow and flood stage (Figure 10). At bankfull the distribution is noticeably skewed towards the direction of positive C(Ws, Zs) (i.e., positive sloping linearity), which supports out hypothesis.

In partly confined ephemeral rivers, the character of Ws-Zs distributions is different between the two river types (Figure 10). River type 2 (partly confined, high W/D ratio,

split-channel) has roughly Gaussian Ws-Zs distributions at baseflow. In contrast, river type 5 (partly confined, gravel/cobble, riffle-pool) has a baseflow distribution with a notable tear-drop-shaped skew towards negative covariance. Both river type 2 and 5 have bankfull and flood stage Ws-Zs distributions that are notably less organized, but subtly skewed towards positive covariance at flood stage. The observed flood stage skew leads us to reject our hypothesis that river type 2 will have unorganized Ws-Zs heat plots at all water stages.

In valley confined settings, river types 3 and 4 have tightly clustered Ws-Zs distributions with similar skews at each water stage (Figure 10). For both river types the bivariate distributions skew strongly towards negative Ws-Zs covariance at baseflow, show little to no directional skew at bankfull, and at skew towards positive Ws-Zs covariance at flood stage albeit more mildly in river type 4. Results support the prediction that in confined valley settings the structure of fluvial topography is highly flow-stage dependent, and more tightly organized, potentially due to valley walls limiting width variability. This was found to be particularly true at baseflow, where high bed elevation co-occurs frequently with relative width constrictions in a linear like fashion.

3.3 **O1c.** How do the relative abundances of flow convergence routing landforms across stages and river types?

Average landform relative abundances were found to be significantly non-uniform at baseflow for river types 3, 4, and 5 (ANOVA $p < 0.05$). In each case nozzle and oversized cross-sections (-Ws-Zs covariance) were more prevalent than constricted

pool and wide bars cross-sections (+ Ws-Zs covariance). This matched the hypothesis. However, we also predicted that river types 1 and 2 would similarly exhibit negative covariance landforms at baseflow, which was visually observable (Figure 11) but not statistically significant. At bankfull stage, only the valley confined river types 3 and 4 had statistically significant non-uniform landform relative abundances ($p < 0.05$ level). For both negative covariance landforms were still more prevalent, albeit by lesser margins than at baseflow. At flood stage, river types 2 and 3 had statistically significant non-uniform relative landform abundances ($p < 0.05$), characterized for both by a scarcity of nozzles and a higher abundance of wide bars and constricted pools.

The ANOVA test applied to compare landform relative abundances between river types found significant variability in only two cases. Baseflow wide bars are significantly more common in river types 1 and 2 (mean=9.3%). Bankfull nozzles are significantly more common in both confined river types 3 and 4. The prediction that positive covariance landforms would be significantly more abundant for river type 5 was not supported by results. However, the prediction that negative covariance landforms would be more abundant in confined river types at non-baseflow stages than other river types was found to be somewhat true at least for bankfull nozzles.

Finally, in all river types, the relative abundance of oversized cross-sections (+Ws, -Zs) remained relatively constant across water stages. In river types 1, 2, and 5 the flow-stage variability of all other non-normal landform relative abundances was not significant at the $p < 0.05$ level. In confined river types 3 and 4, the non-oversized, landforms vary in abundance significantly ($p < 0.05$) across water stages. In both river

types, the relative abundance of wide bars and constricted pools (+ Ws-Zs covariance) increases with flow-stage, contrasted to nozzles which half in abundance across both baseflow to bankfull, and bankfull to flood-stage transitions (Figure 11).

3.4 **O2a.** Are relative topographic highs and lows at baseflow and bankfull associated with width undulations occurring at bankfull and flood stage topography respectively?

In river types 1, 2, 4, and 5 cross-sections with high bed elevation ($Zs > 0.5$) at baseflow had significantly greater mean widths at bankfull than cross-sections with low bed elevation ($Zs < -0.5$) at baseflow ($p < 0.05$). This trend was particularly pronounced for unconfined river type 1 that had a mean bankfull Ws associated with baseflow topographic highs that was 0.69 standard deviations greater than the topographic lows (Figure 12). In contrast, river type 3 cross-sections with $Zs > 0.5$ have a mean Ws value that is 0.18 lower than cross-sections with $Zs < -0.5$. This analysis largely supported the prediction that baseflow topographic highs would be associated with higher bankfull width than baseflow topographic lows, however river type 3 was the exception.

In all river types except type 2, cross-sections with high bed elevation at bankfull had a mean flood-stage Ws that was significantly greater than cross-sections with low bed elevation at bankfull stage, again with river type 1 having the largest discrepancy. River type 2 mean Ws values at flood stage did not differ at the $p < 0.05$ significance level. The hypotheses that bankfull-to-flood stage preferential nesting would be observed exclusively in the more non-uniform river types 3 and 5 was not supported.

3.5 **O2b.** Do flow convergence routing landforms have preferred nesting structures (i.e., baseflow nozzles within bankfull wide bars)?

Results indicated that preferential flow convergence routing landform nesting structures exist and can be meaningfully interpreted. Significance levels for all Chi-Squared tests were exceedingly high. Therefore, landform transitions between stages cannot be explained by landform relative abundances alone. This supports the notion that nested stage-dependent fluvial landforms are not independent of each other. In all river types, the most strongly overrepresented nesting structure is one where landform designation remains constant at all three stages. We found that for all river types baseflow nozzles are preferentially nested within bankfull wide bars, which supports predictions and the expectations of flow convergence routing theory. We also found that wide bars are ubiquitously preferentially nested within oversized cross-sections in both flow-stage transitions. Additionally, unconfined and partly confined river types 1, 2, and 5, had baseflow oversized cross-sections preferentially nested within bankfull constricted pools. This preferential nesting structure was observed as well in river type 5 (Figure 13b) going from bankfull-to-flood stage, potentially contributing to the class's riffle-pool morphology. However, broadly our hypothesis that bankfull to flood-stage preferential nesting structures would be limited to river types 3 and 5 was incorrect.

A handful of channel-type-specific preferred nesting structures were observed as well. River type 1 (Figure 13a) baseflow nozzle cross-sections were preferentially nested within bankfull wide bars. Bankfull constricted pools are preferentially nested within flood stage nozzles at more than twice the expected frequency. In addition, river type 2

bankfull nozzles were preferentially nested within flood stage constricted pools, and vice-versa, with constricted pools at bankfull preferentially nested within flood stage nozzles.

4 Discussion

4.1 Unconfined fluvial topography is organized at bankfull

On average, we find that ephemeral rivers in unconfined corridors have Ws and Zs longitudinal patterning at bankfull that strongly match the predictions of flow convergence routing theory in a two-stage mode. Unlike in partly confined (types 2 and 5) and confined (types 3 and 4) river types, unconfined river type 1 Ws and Zs series do not coherently covary (Table 3) at either baseflow or flood-stage. The lack of such coherence at flood stage was predicted; in an unconfined setting, floodplain, terrace, or valley hillside width undulation would only steer flow in a highly dispersed state (given the high cross-sectional area) with little channel-altering potential. In contrast, at bankfull stage unconfined reaches have a high bankfull mean C(Ws, Zs) value of 0.38, with on average more than 60% of cross-sections having positive Ws·Zs covariance (Table 3). This suggests that flow convergence routing plays a dominant role at bankfull discharge exclusively and self-organizes longitudinal fluvial topography without confining valley input. In addition, baseflow topographic highs and lows (see question O2a) are more strongly associated with bankfull wide and narrow intervals, respectively, than in any other river type (Figure 12). We conclude that in unconfined settings bankfull scale width undulations largely control in-channel sedimentary dynamics via the flow

convergence routing mechanism.

4.2 Riffle-pool channel morphology in partly confined ephemeral rivers is likely maintained by bankfull morphology topographic steering

Flow convergence routing theory was originally developed to explain the self-maintenance of riffle-pool channel morphology in alluvial rivers, a morphology that provides desirable salmonid habitat (Hamann et al., 2014). This generalizes classical velocity reversal theory (Keller, 1971) that predicts that riffle-pool morphology is maintained by a reversal in peak velocity from riffles to pools as discharge increases from baseflow to bankfull. How flow convergence routing theory would apply in different climates and river types has not been thoroughly studied. A lot of work has been done on gravel and cobble bedded streams in temperate and semiarid partly confined rivers (Sawyer et al., 2010; White et al., 2010; Gervasi et al., 2021).

In evaluating flow convergence routing across five river types with ephemeral hydrology, the theory is largely supported by our sample of partly confined, riffle-pool rivers. The study reaches typically switch dramatically from having negative covariance baseflow GCS, to positive covariance bankfull GCS (see question O1a). Mean C(Ws, Zs) transitions from -0.35 at baseflow to 0.28 at bankfull, a statistically significant increase of 0.63. In contrast, river type 2, also with a partly confined valley setting, has a similar mean bankfull C(Ws, Zs) value but experiences a nearly half as small, non-statistically significant 0.35 increase in mean C(Ws, Zs). This suggests that while bankfull scale width appears to somewhat control channel bed elevation in partly confined rivers

broadly, riffle-pool channel morphology may specifically be a product of the observed Ws·Zs covariance sign reversal going from baseflow to bankfull.

Using landform cross-sectional area as a proxy for velocity, and our landform transition analysis (see question O2b), we can see that flow convergence routing theory's prediction is supported. That is, baseflow nozzles (flow convergence, high velocity) are preferentially nested within bankfull wide bars (flow divergence, low velocity), and baseflow oversized cross-sections (flow divergence, low velocity) are preferentially nested within bankfull constricted pools (flow convergence, high velocity). River type 5's preferential landform nesting structure is visualized using a Sankey diagram (Figure 13b). The strong association leads to the conclusion that bankfull channel width undulations, given suitable sediment supply, can topographically steer bankfull and flood flows, thereby likely maintaining bed relief and the desirable riffle-pool riverine habitat associated with it (Hamann et al., 2014).

We cannot ascertain which discharge magnitudes are dominating the process in collaboration with bankfull channel topography. It is possible that bankfull flow is sufficient, though Shields stress evaluations have cast doubt on that for gravel and cobble bedded rivers (Pasternack et al., 2018b, 2021). It is also possibility that flood flows control both baseflow and bankfull topography simultaneously. Finally, it possible that flood flows control bankfull topography at flood peaks, and then in turn on the falling limb of a flood, bankfull topography drives topographic steering and morphodynamics of the nested baseflow topography. Detailed hydrodynamic and morphodynamic studies are needed to continue to investigate these possibilities (Sawyer et al., 2010; Strom et

al., 2016).

4.3 In valley confined settings, flow convergence routing's relevance increases with discharge

Valley confined river reaches have been previously characterized by a 'Pool Expansion Riffle Contraction' (PERC) configuration, which describes a setting where narrow cross-sections tend to be shallow, and wide cross-sections tend to be deep (Jaeger et al., 2017; Mohadevi et al., 2021). Generally, the configuration's counter-intuitive stability is not self-generated by internal dynamics but rather imposed by width-restricting, elevation-increasing hillslope debris flows, resistant bedrock outcrops, and the scour potential associated with large boulders (Jaeger et al., 2017).

We find with ephemeral hydrology this traditional characterization of valley-confined longitudinal topography exists predominantly at baseflow and is altered as stage increases. In both confined river types (river types 3 and 4), mean C(Ws, Zs) at baseflow is strongly negative (Table 3) and there is a high relative abundance of nozzle and oversized landforms (Figure 11). The baseflow bivariate Ws, Zs distributions (Figure 10) visualize the skew towards negative Ws-Zs covariance, and for river type 3 specifically, display a surprising level of 2D organization given the volume of cross-sections studied (see question O1b). In contrast to other river types where flood stage mean C(Ws, Zs) is comparable or less than bankfull, in confined settings mean C(Ws, Zs) increases with stage. Despite this, the 'PERC' configuration description of mountain rivers (Mohadevi et al., 2021), as represented here by negative C(Ws, Zs), generally

ignores the flow-dependent nature of confined setting fluvial topography. This may be related to the difficulty of gathering field data in confined mountain rivers at flashy high flows, and potentially is an example of how 1-m scale topo-bathymetric DEMs can contribute to our broadly fieldwork-based understanding of fluvial geomorphology.

Our analysis suggests that in contrast to other river types, in the valley confined river types, flow convergence routing's relevance as a morphodynamic mechanism is broadly limited to and depends on floods- often very large ones. Bankfull inundated topography appears to exist in a transition between negative and positive C(Ws, Zs) channel configurations (Table 3), and in river type 3 specifically, has no relationship to baseflow bed elevation undulations (see question O2a). At flood stage, both confined river types have positive mean C(Ws, Zs) values (Table 3), with the percent of cross-sections on average with positive Ws-Zs covariance near 60%.

We notice that the described baseflow-to-flood stage increase in mean C(Ws, Zs) is of significantly greater magnitude, and occurring at higher stages, for river type 3 than river type 4. This strong suggests that, as hypothesized, sediment size plays a key role in determining at what discharge flow convergence routing begins to define channel dimensions (Jackson et al., 2015; Bayat et al., 2017). Rivers of type 3 and 4 all exist in South Coast mountains, which are characterized by high volumes of stochastically injected, poorly sorted, sediment driven by colluvial hillslope processes (Inman & Jenkins, 1999).

In a hypothetical setting with a uniform sediment size distribution, flow convergence

routing could suddenly become relevant above the specific discharge capable of mobilizing said sediment size. In such a case, we would expect to see channel topography favoring positive C(Ws, Zs). Yet in our confined river reaches, especially ones with cobble-boulder sediment regimes (river type 3), we do not see such threshold-like behavior as was found for Pasternack et al. (2021). One possible explanation is the use of only three Zd stages in this study, whereas Pasternack et al. (2021) used seven, of which four were flood stages. Alternately, it could be more related to the very high sediment supply and unregulated flow regime of South Coast ephemeral streams in California, compared to the high-elevation, high precipitation setting of Pasternack et al. (2021). Therefore, in reaches with high fluxes of very coarse sediment, flow convergence routing may become continuously more relevant as flood stage rises further. Another possibility is that a confining valley wall's ability to drive sedimentary dynamics is inversely proportional to its distance from the thalweg, because a proximal valley wall steers flow that is less laterally dispersed, and therefore at higher energy state. In conclusion, valley-confined river baseflow channels with ephemeral hydrology can broadly be characterized by the negative C(Ws, Zs) cross-sectional dimensions. Yet larger scale sedimentary dynamics appear to require and be driven by the highest discharges via flow convergence routing, potentially as a function of the sediment size distribution or valley wall distance.

4.4 Sources of uncertainty

There are two main sources of uncertainty effecting our study's findings: DEM derived

uncertainty and methodological uncertainty. The former largely results from technical limitations associated with airborne LiDAR bare-earth terrain modeling, while the latter is driven by portions of our methodology that required subjective input.

4.4.1 DEM uncertainty

GCS analysis is completely derived from fluvial DEMs, so DEM accuracy is critical to our findings. Accuracy in this case is not so much about the absolute deviation between real and modeled elevations, but simply whether extracted cross-sectional average bed elevation and top width end up in the correct bin for FCR landform classification. Thus, GCS analysis involves substantial reduction of uncertainty via decision-tree binning. That leaves the accuracy of DEM values close to decision thresholds most vulnerable to propagating error. Whether fuzzy rulesets would improve handling of uncertainty more that it would add confusion via seemingly arbitrary fuzzy rules and difficulty for users unsatisfied with applying percent likelihoods depends on one's comfort level with those tools and products. Fuzzy rulesets could at least help identify the most uncertain cross-sections.

Standardized DEM field validation using independent ground-based methods is possible when a site is close by, but as science expands to studying larger regions, even whole continents, validation would be a costly and time-consuming affair. Thus, DEM error is not able to be explicitly estimated and must be discussed in terms of uncertainty. Past literature documents two sources of error afflicting DEMs derived from LiDAR data: random error and systematic error (Fisher & Tate, 2006). Random error is introduced by

significant terrain noise at a scale smaller than the DEM resolution (1m). For example, LiDAR returns may randomly only capture a boulder or woody element embedded into lower lying sediments and assign the 1m raster cell an erroneously high elevation value. Random error is estimated at the LiDAR project level using RMSE (see Table 2 for values) but is potentially underestimated in sampled reaches with coarse (cobble-boulder), poorly sorted, sediments.

Systematic error is introduced by LiDAR point cloud processing and the conversion to a 1m resolution DEM. LasTools (Hug et al., 2004) provides powerful algorithms that remove LiDAR returns representing vegetation, ideally leaving point clouds characterizing only bare-ground topography. In practice, these algorithms require parameter tuning (see supplementary materials), and their effectiveness depends on the LiDAR data quality and nature of riparian vegetation. Specifically, low-lying shrubby vegetation species can contribute to poor vegetation point removal, resulting in erroneously high DEM cell values (Norheim et al., 2002; Gould et al., 2013). All DEMs were closely inspected for quality and re-processed with adjusted parameters, when necessary, but some vegetation induced systematic error is unavoidable. Vegetation induced error increases with slope regardless of dominant species (Gould et al., 2013), therefore systematic error may be more prevalent in the confined, mountainous, vegetated reaches. In addition, systematic error can be introduced by any of the common point cloud interpolation techniques used to generate DEMS, which inherently discretize continuous topographic variability into 1m scale elevation values. Choice of interpolation technique likely does not affect average elevation error (Fisher & Tate,

2006), therefore in topographically noisier settings averaging to the 1m cell scale may unavoidably obscure some hydro-morpho dynamically relevant aspects of topography.

4.4.2 Methodological uncertainty

Methodological uncertainty is introduced at all steps where subjectivity was required given the lack of field validation and sample diversity. We used linear piecewise regression on thalweg elevation profiles to detrend topo-bathymetric DEMs (see section 25), a process that requires slope-break points to be manually identified. In practice, this is a highly subjective, iterative process; slope breakpoints are first chosen based on visual analysis of the elevation profile, then the resulting piecewise regression fit is analyzed for suitability, which enables further breakpoint selection refinement. Selecting too many breakpoints can over-fit the longitudinal elevation profile, obscuring relevant topographic undulations in the resulting detrended DEM. On the other hand, in a setting with significant changes in slope, underfitting the elevation profile produces a detrended DEM where cell elevation values are skewed by valley scale trends not relevant to our hydro-morphodynamic interpretation.

Key Zd stage selection was another step defined by subjectivity, and potentially introduced systematic error challenging the comparisons made between river types at ‘analogous’ water stages heights. Slovin (2015) suggests that remotely sensed bankfull wetted area estimations result in a 6% greater mean bankfull width than when measured in the field. Given the different techniques required by each river type to delineate key water stages (see section 2.4), it is plausible that the key Zd stages were

systematically defined in meaningfully different ways between river types. Yet given the morphological diversity within our sample, whether two Zd stages in different settings can truly be deemed ‘analogous’ in the first place remains uncertain. Despite the inherent uncertainties associated with studying complex fluvial topographies using remote sensing data, we believe that our novel comparisons made between river types remain valuable and broadly replicable within a margin of error. With the automated GCS software in hand now, it is feasible to analyze many Zd stages in future studies, and then either figure out objective rules for selecting ones to prioritize or develop new metrics for evaluating them comprehensively.

4.5 Potential improvements

4.5.1 Expanding the scope of GCS analysis

While our study provides novel scientific and methodological contributions that build on existing conceptualizations of hydro-morphodynamic processes (Keller, 1971; White et al., 2010; Pasternack et al., 2018a), expanding the scope of GCS analysis could generate findings with more direct management applications. We studied ephemeral river reaches because of data availability, but as access to airborne green-LiDAR data expands, similar topo-bathymetric analysis could be conducted on previously unmapped perennial river reaches. Perennial riverine habitat has received far more attention and restoration funds than their ephemeral counterparts (Bernhardt & Palmer, 2011; Datry et al., 2017). Further characterizing flow convergence routing’s role as a mechanism for maintaining perennial riverbed elevation undulations, which can sustain desirable

freshwater habitat (Reid et al., 2019; Duffin et al., 2021), could significantly contribute to river restoration design and flow regulation literature. In addition, quantitatively comparing the hydro-morphodynamics of otherwise similar perennial and ephemeral rivers would be a novel scientific contribution to fluvial geomorphology in and of itself.

Future research could apply GCS analysis across a topographic time series, potentially characterizing the topographic drivers of observed longer-term fluvial morphology. Flow convergence routing theory describes a hydro-morphodynamic mechanism responsible for some proportion of channel bed evolution. Despite its advantage of directly conceptually linking current longitudinal fluvial topography and expected patterns of deposition and scour, research explicitly comparing expected and observed long-term channel morphodynamics via GCS analysis has been limited to the Yuba River, CA (Pasternack et al, 2021). Hydrology-topography interactions could be more directly observed by combining GCS analysis with DEM differencing (James et al., 2012), and when available, discharge gage data. Currently, such a study would be limited in scale by the shortage of fluvial topo-bathymetric data, especially over longer time periods (Kinzel et al., 2013; Lague & Feldmann, 2020). As data availability and analysis techniques advance, the field of fluvial geomorphology has the potential to make and test more specific morphodynamic predictions over larger, more diverse samples of river reaches.

4.5.2 Underlying factors supporting width variability

Both landforms expected to be freely forming in flow convergence routing theory, wide

bars, and constricted pools, have been shown to be driven by width undulation forced vertical deposition and scour (Byrne et al., 2021). Yet the factors maintaining said width undulations have not been as extensively studied as the topographic variability they can produce. Future research could investigate these underlying factors and contribute to implementing resilient river restoration designs (Palmer & Ruhi, 2019). Such factors are likely diverse products of specific environments, and despite potentially maintaining similar width variability, can be very different depending on channel setting. Some factors that may contribute to long-term longitudinal width variability are outcropping bedrock (Jaeger et al., 2017), frequent debris flows (Gangodagamage et al., 2007), large woody elements (Wohl, 2017), spatially variable soil erodibility (Konsoer et al., 2016), mammalian activity (Beschta & Ripple, 2012), and riparian vegetation (Arnold & Toran, 2018; Vargas-Luna, 2018). Their relationship to longitudinal fluvial topography could be studied explicitly; for example, how does the abundance or type of floodplain vegetation present affect bankfull width variability.

4.5.3 Moving past river type classification?

Our study used a river-type classification system (Byrne et al., 2020a) to group sampled river reaches, and interpreted differences in longitudinal fluvial topography relevant to hydro-morphodynamics. Identifying such differences, and interpreting them, can enable management decisions to be fine-tuned to different river types. However, while conceptual linkages exist between river types and ecosystem services, fluvial geomorphology has the opportunity to move past river type classification systems by

directly quantifying the aspects of channel morphology deemed relevant to specific management efforts. A much-studied example is riffle-pool river types being associated with desirable salmonid habitat (Hamann et al., 2014). Our analysis involves defining a group of river reaches as riffle-pool containing, and then assessing whether their topographic structure is different from other river types in potentially explanatory ways (see section 4.1). Yet the degree to which our sampled ‘riffle-pool’ reaches (river type 5, see Table 1) are similar to each other, or provide suitable riverine habitat, remains unstudied. Recent research has expanded the ability to quantify management relevant aspects of channel morphology from high-resolution DEMs; for example, riffle-pool pairs can be automatically identified using a wavelet analysis (Duffin et al., 2021), and suitable habitat area can be plotted as a function of discharge using 2D modeling approaches (Theodoropoulos et al., 2020). Rather than quantifying how a riffle-pool river type class may or may not have statistically different GCS values, future research could explicitly explore the relationship between GCS and the number of riffle-pool pairs present in a reach, a habitat suitability index, wood abundance, and other relevant metrics.

5 Conclusions

To assess whether a large sample of ephemeral rivers exhibit geomorphic differences between river types and as a function of stage we generated 35 1-m resolution topo-bathymetric DEMs of morphologically diverse ephemeral river reaches in the South Coast region of California. Broadly, we found that geomorphic covariance analysis

applied regionally can help identify the role specific hydro-morphodynamic mechanism plays in different river types. GCS methodology produces longitudinal standardized width (Ws) and standardized, detrended bed elevation (Zs) series at three key water stages. We analyzed these series to interpret fluvial topography in relation to a known hydro-morphodynamic mechanism, flow convergence routing. We found that all river types have longitudinal fluvial topographic structures that significantly differ across three key water stages, which in some cases facilitated coherent hydro-morphodynamic interpretations. Applying our findings to a flow regulation context, we suggest that releasing bankfull discharge flows is necessary to maintain riffle-pool habitat, with the specific duration required up for local determination. In a river restoration design context, our findings suggest that constructing resilient bankfull scale width undulations is likely to induce freely forming in-channel bed undulations. Additionally, we provide a proof-of-concept for future high-resolution DEM based, larger sample size, fluvial geomorphology research at regional to global scales.

6 Acknowledgments

This research was supported by the California State Water Resources Control Board under grant number 16-062-300. The authors also acknowledge the USDA National Institute of Food and Agriculture, Hatch project numbers #CA-D-LAW-7034-H and CA-D-LAW-2243-H. We thank Prof. Mark Grismer and Dr. Anzy Lee for input and reviews.

7 References

Abatzoglou, J. T., Redmond, K. T., & Edwards, L. M. (2009). Classification of regional climate variability in the state of California. *Journal of Applied Meteorology and Climatology*, *48*(8), 1527–1541. https://doi.org/10.1175/2009JAMC2062.1

Baartman, J. E. M., Masselink, R., Keesstra, S. D., & Temme, A. J. A. M. (2013). Linking landscape morphological complexity and sediment connectivity. *Earth Surface Processes and Landforms*, *38*(12), 1457–1471. https://doi.org/10.1002/esp.3434

Bayat, E., Rodríguez, J.F., Saco, P.M., De Almeida, G.A., Vahidi, E. & García, M.H., (2017). A tale of two riffles: Using multidimensional, multifractional, time-varying sediment transport to assess self-maintenance in pool-riffle sequences. *Water Resources Research*, *53(3)*, 2095–2113.

Billi, P., Demissie, B., Nyssen, J., Moges, G., & Fazzini, M. (2018). Meander hydromorphology of ephemeral streams: Similarities and differences with perennial rivers. *Geomorphology*, *319*, 35–46. https://doi.org/10.1016/j.geomorph.2018.07.003

Brown, R. A., Pasternack, G. B. (2014). Hydrologic and topographic variability modulate channel change in mountain rivers. *Journal of Hydrology*, 510, 551-564. https://doi.org/10.1016/j.jhydrol.2013.12.048

Brown, R. A., Pasternack, G. B., Lin, T. (2015). The topographic design of river channels for form-process linkages for river restoration. *Environmental Management*, 57 (4), 929-942. https://doi.org/10.1007/s00267-015-0648-0

Brown, R. A., & Pasternack, G. B. (2017). Bed and width oscillations form coherent patterns in a partially confined, regulated gravel-cobble-bedded river adjusting to anthropogenic disturbances. *Earth Surface Dynamics*, *5*(1), 1–20. https://doi.org/10.5194/esurf-5-1-2017

Bull, L. J., Kirkby, M. J., Shannon, J., & Hooke, J. M. (2000). The impact of rainstorms on floods in ephemeral channels in southeast Spain. *Catena*, *38*(3), 191–209. https://doi.org/10.1016/S0341-8162(99)00071-5

Byrne, C. F., Guillon, H., Lane, B. A., Pasternack, G. B., & Sandoval-Solis, S. (2020a). *Coastal California Regional Geomorphic Classifications*. California State Water Resources Control Board.

Byrne, C. F., Pasternack, G. B., Guillon, H., Lane, B. A., & Sandoval-Solis, S. (2020b). Reach-scale bankfull channel types can exist independently of catchment hydrology. *Earth Surface Processes and Landforms*, *45*(9), 2179-2200. https://doi.org/10.1002/esp.4874

Byrne, C. F., Pasternack, G. B., Guillon, H., Lane, B. A., & Sandoval-Solis, S. (2021). Channel constrictions predicts pool-riffle velocity reversals across landscapes. *Geophysical Research Letters*, *48*(20). https://doi.org/10.1029/2021GL094378

Caamaño, D., Goodwin, P., Buffington, J. M., Liou, J. C. P., & Daley-Laursen, S. (2009). Unifying criterion for the velocity reversal hypothesis in gravel-bed rivers. *Journal of Hydraulic Engineering*, *135*(1), 66–70. https://doi.org/10.1061/(ASCE)0733-9429(2009)135:1(66)

Carson, M. A. (1984). The meandering-braided river threshold: a reappraisal. *Journal of Hydrology*, *73*(3-4), 315-334. https://doi.org/10.1016/0022-1694(84)90006-4

Cavalli, M., Tarolli, P., Marchi, L., & Dalla Fontana, G. (2008). The effectiveness of airborne LiDAR data in the recognition of channel-bed morphology. *Catena*, *73*(3), 249–260. https://doi.org/10.1016/j.catena.2007.11.001

Clubb, F. J., Mudd, S. M., Milodowski, D. T., Valters, D. A., Slater, L. J., Hurst, M. D., & Limaye, A. B. (2017). Geomorphometric delineation of floodplains and terraces from objectively defined topographic thresholds. *Earth Surface Dynamics*, *5*(3), 369–385. https://doi.org/10.5194/esurf-5-369-2017

Datry, T., Bonada, N., Boulton, A. J. (2017). Chapter 1 - General Introduction. In: Datry, T., Bonada, N., & Boulton, A. (Eds.) *Intermittent Rivers Ephemer. Streams*, 1-20. https://doi.org/10.1016/B978-0-12-803835-2.00002-4

De Almeida, G. A. M., & Rodríguez, J. F. (2012). Spontaneous formation and degradation of pool-riffle morphology and sediment sorting using a simple fractional transport model. *Geophysical Research Letters*, *39*(6), 1–7. https://doi.org/10.1029/2012GL051059

De'ath G, Fabricius K.E. (2000). Classification and regression trees: a powerful yet simple technique for ecological data analysis. *Ecology,* 81, 3178-3192. https://doi.org/10.1890/0012-9658(2000)081[3178:CARTAP]2.0.CO;2

Dettinger, M. D., Ralph, F. M., Das, T., Neiman, P. J., & Cayan, D. R. (2011). Atmospheric rivers, floods and the water resources of California. *Water, 3*(2), 445–478. https://doi.org/10.3390/w3020445

Erskine W. D & Livingstone E. A. (1999). In-channel benches: the role of floods in their formation and destruction on bedrock confined rivers. In: Miller A. J., & Gupta A (Eds.) *Varieties of Fluvial Form*. John Wiley and Sons, New York, 445–475.

ESRI. (2011). ArcGIS Pro Desktop: Release 2.4. Redlands, CA: Environmental Systems Research Institute.

Gangodagamage, C., Barnes, E., & Foufoula-Georgiou, E. (2007). Scaling in river corridor widths depicts organization in valley morphology. *Geomorphology*, *91*(3–4), 198–215. https://doi.org/10.1016/j.geomorph.2007.04.014

Gervasi, A. A., Pasternack, G. B., East, A. E. (2021). Flooding duration and volume more important than peak discharge in explaining 18 years of gravel-cobble river change. *Earth Surface Processes and Landforms*. https://doi.org/10.1002/esp.5230

Gould, S. B., Glenn, N. F., Sankey, T. T., & McNamara, J. P. (2013). Influence of a Dense, low-height shrub species on the accuracy of a lidar-derived DEM. *Photogrammetric Engineering and Remote Sensing*, *79*(5), 421–431. https://doi.org/10.14358/PERS.79.5.421

Gray, A. B., Pasternack, G. B., Watson, E. B., Warrick, J. A. & Goni, M. A. (2015). The effect of El Nino Southern oscillation cycles on the decadal scale suspended sediment behavior of a coastal dry-summer subtropical catchment. *Earth Surface Processes and Landforms*, 40, 272-284. https://doi.org/10.1002/esp.3627

Guillon, H., Byrne, C. F., Lane, B. A., Sandoval Solis, S., & Pasternack, G. B. (2020). Machine learning predicts reach-scale river types from coarse-scale geospatial

data in a large river basin. *Water Resources Research*, *56*(3), 1–22. https://doi.org/10.1029/2019WR026691

Hamann, E. J., Kennedy, B. P., Whited, D. C., & Stanford, J. A. (2014). Spatial variability in spawning habitat selection by chinook salmon (Oncorhynchus tshawytscha) in a wilderness river. *River Research and Applications*, *30*(9), 1099–1109. https://doi.org/10.1002/rra.2704

Hill, R. A., Marc H. W., Scott G. L., Anthony R. O., & Darren J. T. (2016). The stream-catchment (StreamCat) dataset: a database of watershed metrics for the conterminous United States. *Journal of the American Water Resources Association (JAWRA)*, 52, 120-128. https://doi.org/10.1111/1752-1688.12372

Hooke, J. M. (2016). Morphological impacts of flow events of varying magnitude on ephemeral channels in a semiarid region. *Geomorphology*, *252*, 128–143. https://doi.org/10.1016/j.geomorph.2015.07.014

Hug, C., Krzystek, P., & Fuchs, W. (2004). Advanced LiDAR data processing with LasTools. *International Archives of the Photogrammetry, Remote Sensing and Spatial Information Sciences - ISPRS Archives*, *35*(January 2004).

Inman, D. L., & Jenkins, S. A. (1999). Climate change and the episodicity of sediment flux of small California rivers. *Journal of Geology*, *107*(3), 251–270. https://doi.org/10.1086/314346

Jackson, J. R., Pasternack, G. B. & Wheaton, J. M. (2015). Virtual manipulation of topography to test potential pool–riffle maintenance mechanisms. *Geomorphology*, 228, 617-627. https://doi.org/10.1016/j.geomorph.2014.10.016

Jaeger, K. L., Sutfin, N. A., Tooth, S., Michaelides, K., & Singer, M. (2017). Chapter 2.1 - Geomorphology and Sediment Regimes of Intermittent Rivers and Ephemeral Streams. In: Datry, T., Bonada, N., & Boulton, A. (Eds.) *Intermittent Rivers Ephemer. Streams*, 21-49. https://doi.org/10.1016/B978-0-12-803835-2.00002-4

Kasprak, A., Hough-Snee, N., Beechie, T., Bouwes, N., Brierley, G., Camp, R., Fryirs, K., Imaki, H., Jensen, M., O'Brien, G., Rosgen, D., & Wheaton, J. (2016). The blurred line between form and process: a comparison of stream channel classification frameworks. *PLoS ONE*, *11*(3), e0150293. https://doi.org/10.1371/journal.pone.0150293

Keller, E. A. (1971). Areal sorting of bed-load material: The hypothesis of velocity reversal. *Bulletin of the Geological Society of America*, *82*(3), 753–756. https://doi.org/10.1130/0016-7606(1971)82[753:ASOBMT]2.0.CO;2

Kinzel, P. J., Legleiter, C. J., & Nelson, J. M. (2013). Mapping river bathymetry with a small footprint green LiDAR: applications and challenges. *Journal of the American Water Resources Association*, *49*(1), 183–204. https://doi.org/10.1111/jawr.12008

Lague, D., & Feldmann, F. (2020). Chapter 2 -Topo-bathymetric airborne LiDAR for fluvial-geomorphology analysis. In: Tarolli, P., & Mudd, S. M. (Eds.) *Remote Sensing of Geomorphology*, 23, 5-54. https://doi.org/10.1016/B978-0-444-64177-9.00002-3

Lane, B. A., Guillon, H., Byrne, C. F., Pasternack G. B., Rowles, J., Sandoval-Solis, S. (2021). Channel reach morphology and landscape properties are linked across a

large heterogeneous region. *Earth Surface Process and Landforms*. https://doi.org/10.1002/esp.5246

Lane, B. A., Pasternack, G. B., Dahlke, H. E., Sandoval-Solis, S. (2017). The role of topographic variability in river channel classification. *Physical Progress in Geography*, 18. https://doi.org/10.1177/0309133317718133

Lane, B. A., Sandoval-Solis, S, Stein, E. D., Yarnell, S., Pasternack, G. B., Dahlke, H. (2018). Beyond metrics: the role of hydrologic baseline archetypes in environmental water management. *Environmental Management*, 62, 678–693. https://doi.org/10.1007/s00267-018-1077-7

Lowry, R. (2017). Chapter 8 - Chi-Square procedures for the analysis of categorical frequency data. In: Concepts and Applications of Inferential Statistics. Available at: https://web.archive.org/web/20171022032306/http://vassarstats.net:80/textbook/ch8pt1.html

MacWilliams, M. L., Wheaton, J. M., Pasternack, G. B., Street, R. L., & Kitanidis, P. K. (2006). Flow convergence routing hypothesis for pool-riffle maintenance in alluvial rivers. *Water Resources Research*, *42*(10), 1–21. https://doi.org/10.1029/2005WR004391

McKay, L., T. Bondelid, T. Dewald, J. Johnston, R. Moore, and A. and Rea. (2012). NHDPlus Version 2: User Guide. United States Environmental Protection Agency (EPA).

Merritt, A. M., Lane, B., & Hawkins, C. P. (2021). Classification and prediction of natural streamflow regimes in arid regions of the USA. *Water*, *13(3)*, 380. https://doi.org/10.3390/w13030380

Movahedi, N., Dehghani, A. A., Schmidt, C., Trauth, N., Pasternack, G. B., Stewardson, M. J., & Meftah Halghi, M. (2021). Hyporheic exchanges due to channel bed and width undulations. *Advances in Water Resources*, *149*(September 2020), 103857. https://doi.org/10.1016/j.advwatres.2021.103857

Nardini, A., Yépez, S., Mazzorana, B., Ulloa, H., Bejarano, M. D. and Laraque, A. (2020). A systematic, automated approach for river segmentation tested on the Magdalena River (Colombia) and the Baker River (Chile). *Water*, *12*(10), 2827. https://doi.org/10.3390/w12102827

Notebaert, B., Verstraeten, G., Govers, G., & Poesen, J. (2009). Qualitative and quantitative applications of LiDAR imagery in fluvial geomorphology. *Earth Surface Processes and Landforms*, *34*(March), 217–231. https://doi.org/10.1002/esp.1705

Norheim, R. A., Queija, V. R., & Haugerud, R. A. (2002). Comparison of LIDAR and INSAR DEMs with dense ground control. In: *22nd Annual Esri International User Conference,* July 8–12.

Pasternack, G. B. (2011). 2D modeling and ecohydraulic analysis. Createspace: Seattle, WA.

Pasternack, G. B., Baig, D., Weber, M. D., & Brown, R. A. (2018a). Hierarchically nested river landform sequences. Part 1: theory. *Earth Surface Processes and Landforms*, *43*(12), 2510–2518. https://doi.org/10.1002/esp.4411

Pasternack, G. B., Baig, D., Weber, M. D., & Brown, R. A. (2018b). Hierarchically nested river landform sequences. Part 2: bankfull channel morphodynamics governed by valley nesting structure. *Earth Surface Processes and Landforms*, *43*(12), 2519–2532. https://doi.org/10.1002/esp.4410

Pasternack, G. B., Gore, J., & Wiener, J. (2021, submitted). Geomorphic covariance structure of a confined mountain 1 river reveals landform organization stage threshold. *Earth Surface Processes and Landforms*.

Piegay, H., Mathias Kondolf, G., Toby Minear, J., & Vaudor, L. (2015). Trends in publications in fluvial geomorphology over two decades: A truly new era in the discipline owing to recent technological revolution? *Geomorphology*, *248*, 489–500. https://doi.org/10.1016/j.geomorph.2015.07.039

Polade, S. D., Gershunov, A., Cayan, D. R., Dettinger, M. D., & Pierce, D. W. (2017). Precipitation in a warming world: assessing projected hydro-climate changes in California and other Mediterranean climate regions. *Scientific Reports*, *7*(1), 1–10. https://doi.org/10.1038/s41598-017-11285-y

Powell, D. M. (2009). Dryland Rivers: Processes and Forms. In: Parsons A.J., & Abrahams A.D. (Eds) *Geomorphology of Desert Environments*. Springer, Dordrecht. https://doi.org/10.1007/978-1-4020-5719-9_12

Priddy, C. L., & Clarke, S. M. (2020). The sedimentology of an ephemeral fluvial–aeolian succession. *Sedimentology*, *67*(5), 2392–2425. https://doi.org/10.1111/sed.12706

Roth, D. L., Doane, T. H., Roering, J. J., Furbish, D. J., & Zettler-Mann, A. (2020). Particle motion on burned and vegetated hillslopes. *Proceedings of the National Academy of Sciences of the United States of America*, *117*(41), 25335–25343. https://doi.org/10.1073/pnas.1922495117

Sawyer, A. M., Pasternack, G. B., Moir, H. J., & Fulton, A. A. (2010). Riffle-pool maintenance and flow convergence routing observed on a large gravel-bed river. *Geomorphology*, *114*(3), 143–160. https://doi.org/10.1016/j.geomorph.2009.06.021

Scown, M. W., Thoms, M. C. & De Jager, N. R. (2015). Floodplain complexity and surface metrics: Influences of scale and geomorphology. *Geomorphology*, 245, 102-116. https://doi.org/10.1016/j.geomorph.2015.05.024

Segura-Beltran, F., & Sanchis-Ibor, C. (2013). Assessment of channel changes in a Mediterranean ephemeral stream since the early twentieth century. The Rambla de Cervera, eastern Spain. *Geomorphology*, *201*, 199–214. https://doi.org/10.1016/j.geomorph.2013.06.021

Slovin, N. (2015). Using digital elevation models derived from airborne LiDAR and other remote sending data to model channel networks and estimate fluvial geomorphological metrics. *Masters Theses*, *297.* https://doi.org/10.7275/7373499

Strom, M. A., Pasternack, G. B., Wyrick, J. R. (2016). Reenvisioning velocity reversal as a diversity of hydraulic patch behaviors. *Hydrologic Processes*, *30 (13)*, 2348-2365. https://doi.org/10.1002/hyp.10797

Theodoropoulos, C., Stamou, A., Vardakas, L., Papadaki, C., Dimitriou, E., Skoulikidis, N., & Kalogianni, E. (2020). River restoration is prone to failure unless pre-optimized within a mechanistic ecological framework | Insights from a model-based case study. *Water Research*, *173*, 115550. https://doi.org/10.1016/j.watres.2020.115550

Thornbury, W. B. (1954). *Principles of Geomorphology*. Wiley, New York. https://doi.org/10.2134/agronj1954.00021962004600080009x

Warrick, J. A., Hatten, J. A., Pasternack, G. B., Gray, A. B., Goni, M. A., Wheatcroft R.A. (2012). The effects of wildfire on the sediment yield of a coastal California watershed. *Geological Society of America Bulletin*, 124(7-8), 1130-1146. https://doi.org/10.1130/B30451.1

Ward, J. H. (1963). Hierarchical grouping to optimize an objective function. *Journal of the American Statistical Association, 58*(301), 236-44. https://doi.org/10.1080/01621459.1963.10500845

White, J. Q., Pasternack, G. B., & Moir, H. J. (2010). Valley width variation influences riffle-pool location and persistence on a rapidly incising gravel-bed river. *Geomorphology*, *121*(3–4), 206–221. https://doi.org/10.1016/j.geomorph.2010.04.012

Wohl, E. (2017). Bridging the gaps: An overview of wood across time and space in diverse rivers. *Geomorphology*, *279*, 3–26. https://doi.org/10.1016/j.geomorph.2016.04.014

Wohl, E. (2019). Forgotten legacies: understanding and mitigating historical human alterations of river corridors. *Water Resources Research*, *55*(7), 5181–5201. https://doi.org/10.1029/2018WR024433

Wohl, E., & Pearthree, P. (1991). Debris flows as geomorphic agents in the Huachuca Mountains of southeastern Arizona. *Geomorphology*, *4*(3–4), 273–292. https://doi.org/10.1016/0169-555X(91)90010-8

Wohlgemuth, P. M., Beyers, J. L., & Conard, S. G. (1999). Postfire hillslope erosion in southern California chaparral: a case study of prescribed fire as a sediment management tool. *Proceedings of Symposium on Fire Economics, Planning and Policy: Bottom Lines*, *173*, 269–276.

Wyrick, J. R., & Pasternack, G. B. (2016). Revealing the natural complexity of topographic change processes through repeat surveys and decision-tree classification. *Earth Surface Processes and Landforms*, *41*(6), 723–737. https://doi.org/10.1002/esp.3854

Yuen, K. K. (1974). The two-sample trimmed t for unequal population variances. *Biometrika*, 61(1), 165–170. https://doi.org/10.1093/biomet/61.1.165

8 Tables

Table 1. South Coast geomorphic river type descriptions (Byrne et al., 2020a), and their respective sample sizes.

River type	Description	# of river reaches (N)
1	Unconfined, uniform, sand-gravel	6
2	Partly confined, high W/D ratio, split-channel	6
3	Confined, cobble-boulder, cascade/step-pool	7
4	Confined, uniform, gravel-cobble	8
5	Partly confined, riffle-pool, gravel-cobble	8

Table 2. Key metric associated with utilized dry season (May – October) LiDAR project data.

LiDAR dataset	Mean point spacing (m)	Vertical RMSE (cm)	# of river reaches
2015 Los Angeles County, CA QL2 Lidar	0.7	9.95	2
2018 Southern California Wildfire FEMA R9 QL1 Lidar	0.35	10	17
2018 Southern California Wildfire QL2 Lidar	0.7	5.4	16

Table 3. Question O1a. Mean covariance metrics for river reaches within each river type calculated at each flow-stage. Metrics are as follows; mean cross-section covariance (top), and percent of cross-sections with positive C(Ws, Zs) values (bottom).

mean C(Ws, Zs)

	Baseflow		**Bankfull**		**Flood stage**	
River type class	*Mean*	*STD*	*Mean*	*STD*	*Mean*	*STD*
1	-0.09	0.28	0.38	0.22	0.09	0.22
2	-0.07	0.18	0.27	0.47	0.29	0.30
3	-0.52	0.17	-0.02	0.30	0.29	0.16
4	-0.39	0.24	0.10	0.38	0.22	0.34
5	-0.35	0.14	0.28	0.28	0.22	0.35

% C(Ws, Zs) > 0

	Baseflow		**Bankfull**		**Flood stage**	
River type class	*Mean*	*STD*	*Mean*	*STD*	*Mean*	*STD*
1	47.6	12.2	61.5	12.7	59.4	9.8
2	48.9	7.6	59.6	19.3	60.3	11.4
3	29.7	7.2	50.6	9.8	60.7	6.4
4	33.7	11.2	53.5	15.1	57.2	15.3
5	38.3	7.4	58.6	10.3	53.1	19.7

9 Figures

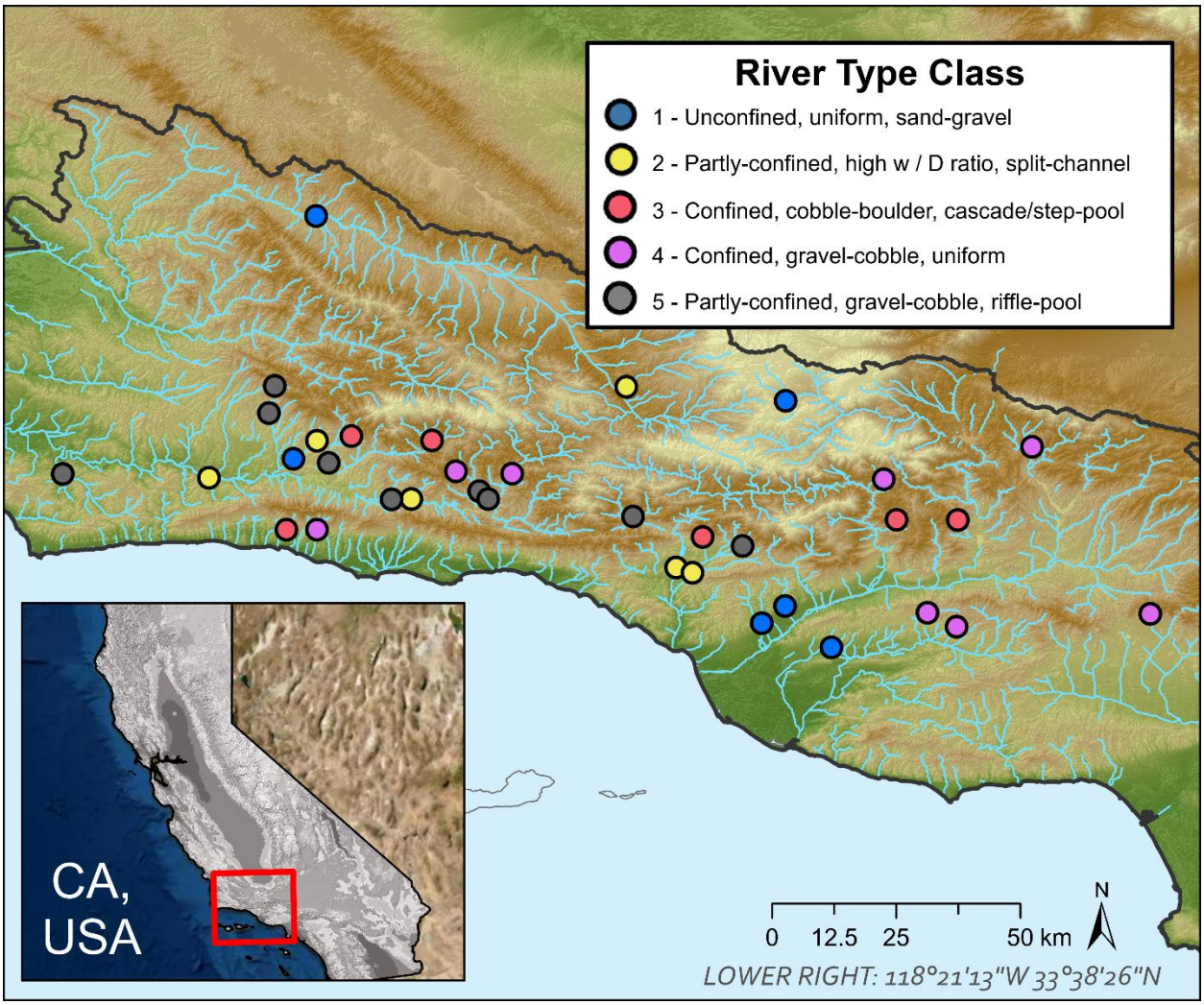

Figure 1. Map of the South Coast showing all sampled river reaches color coded by river type.

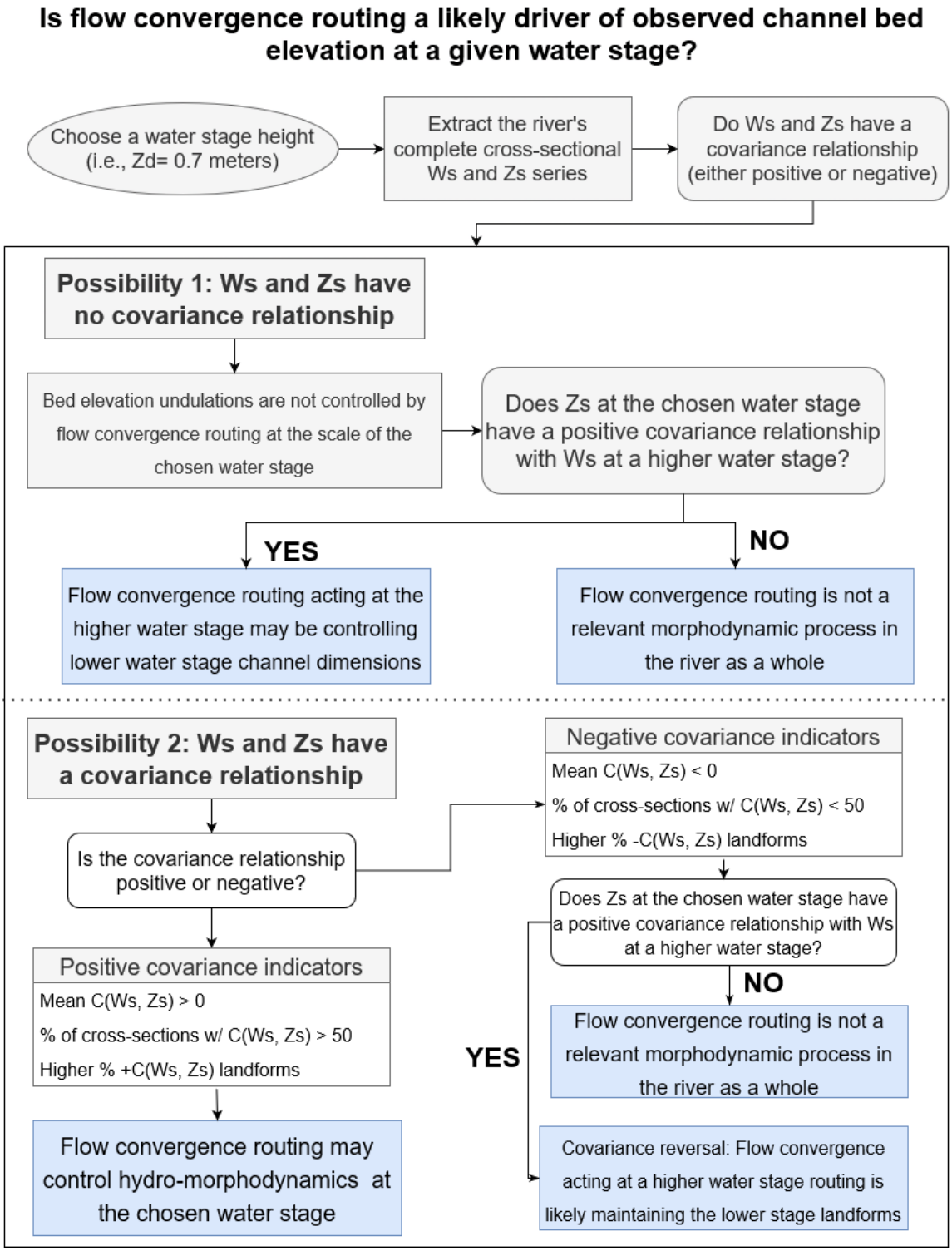

Figure 2. Flow chart showing different possible Ws, Zs covariance relationships, and what they indicate regarding flow convergence routing's potential role as a channel altering fluvial mechanism (shaded blue).

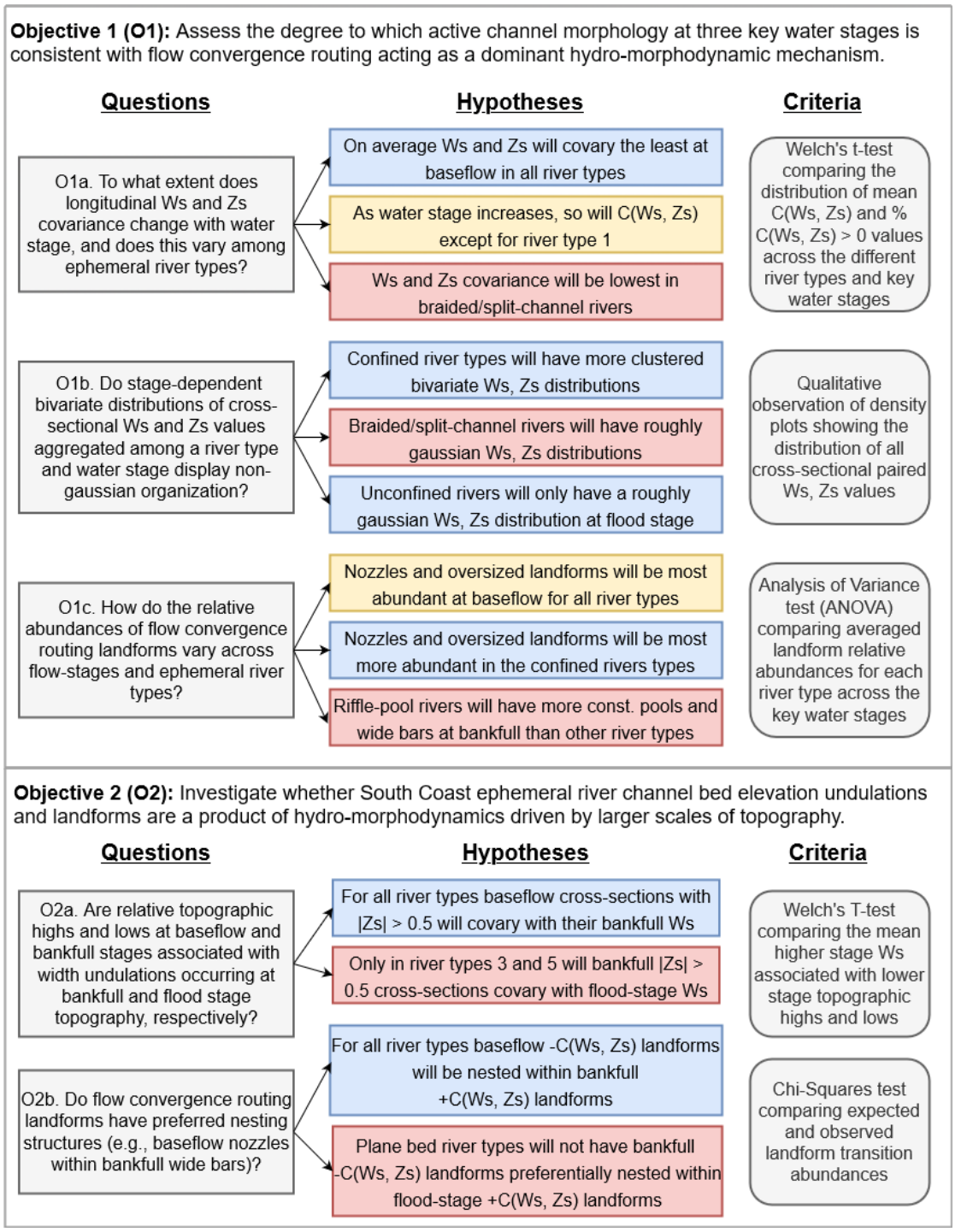

Figure 3. A flow chart displaying both study objectives, their associated questions, as well as our question specific hypotheses and testing criteria. Hypotheses are color coded in relation to our study's findings; blue = hypotheses was supported, yellow = hypothesis was largely supported but with some qualifications, and red = hypothesis was rejected.

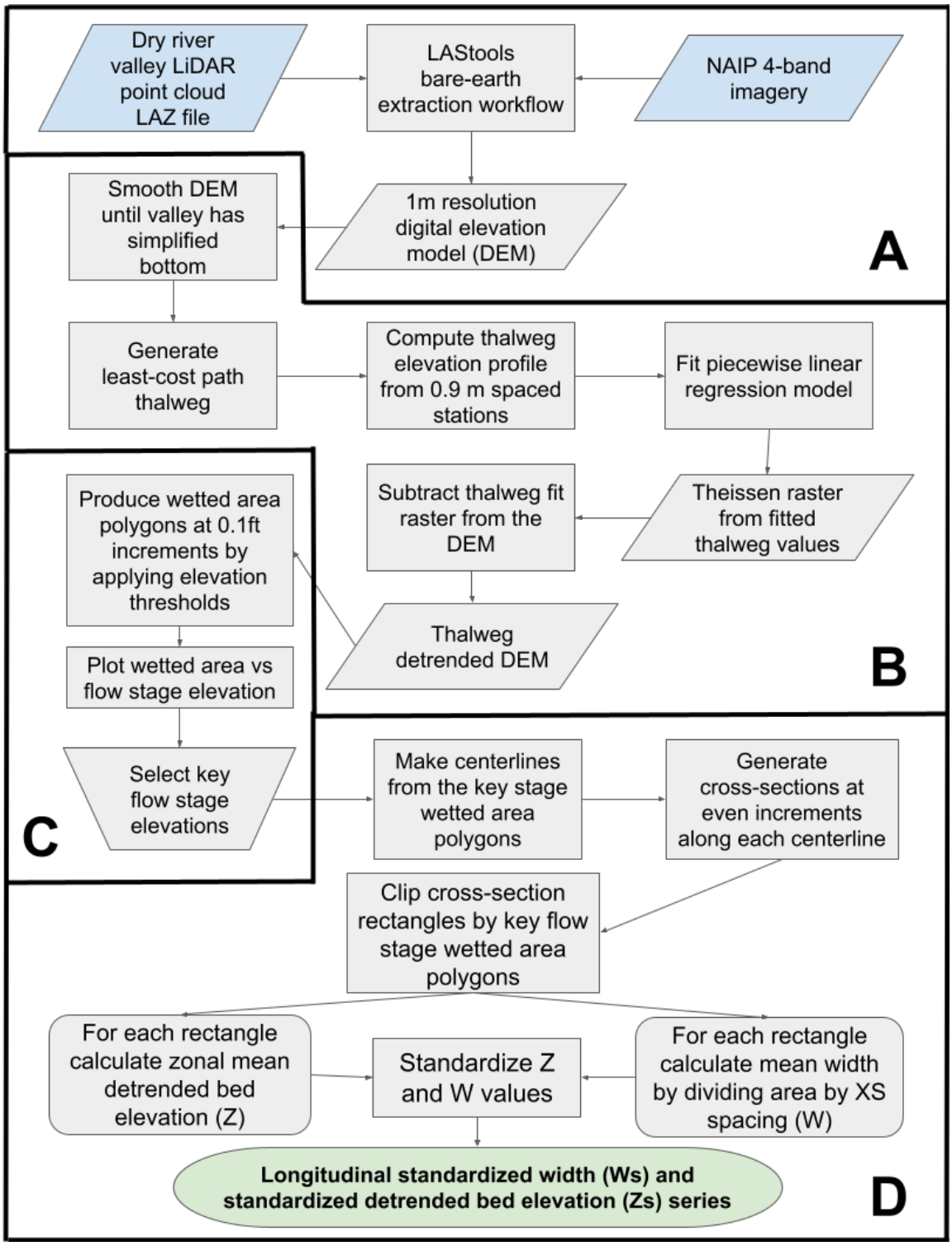

Figure 4. Flow chart showing the LiDAR data processing methodology that outputs baseflow, bankfull, and flood-stage longitudinal standardized width (Ws) and standardized, detrended bed elevation (Zs) series.

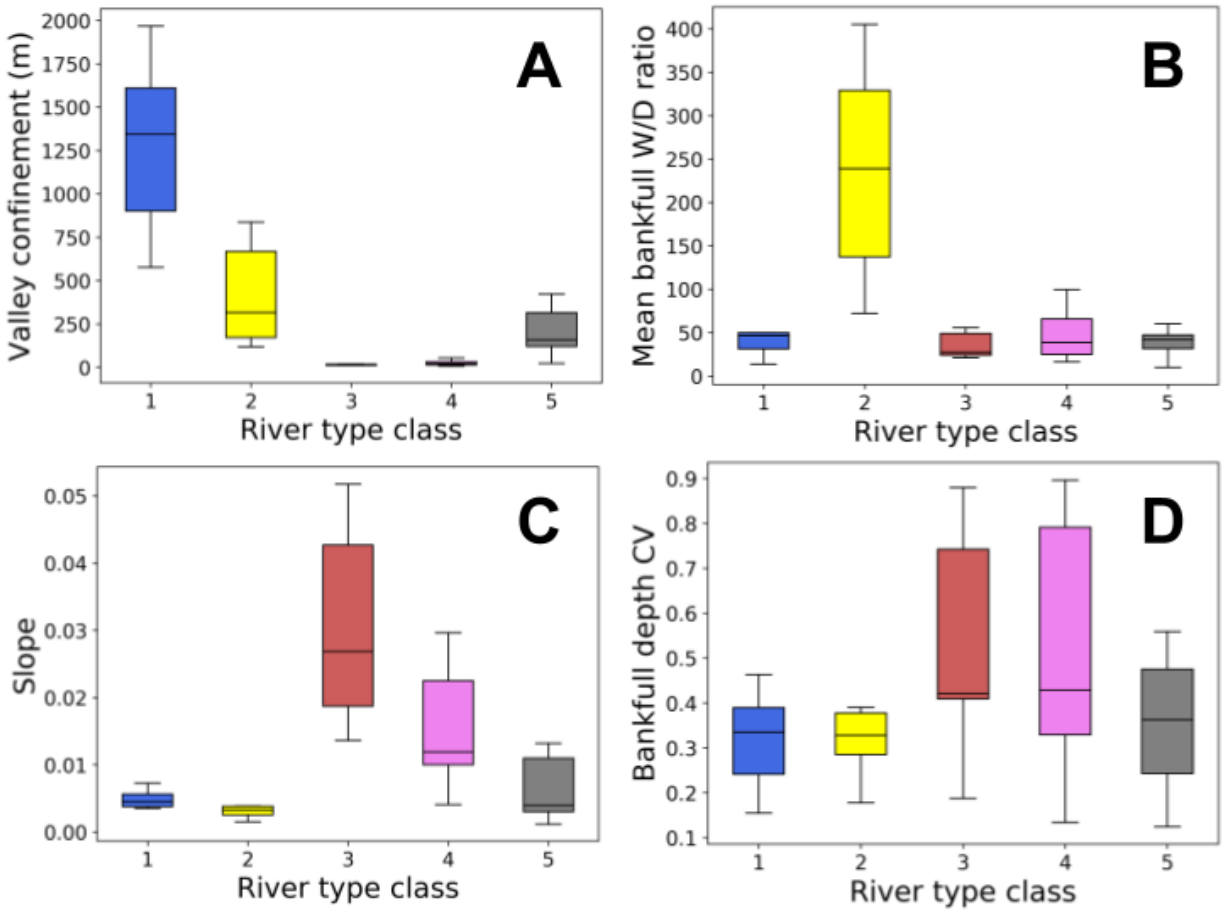

Figure 5. Distribution of valley confinement distance (A), bankfull width to depth ratio B), slope (C), and bankfull depth coefficient of variation (D) values for 5-8 study reaches per river type (35 reaches total).

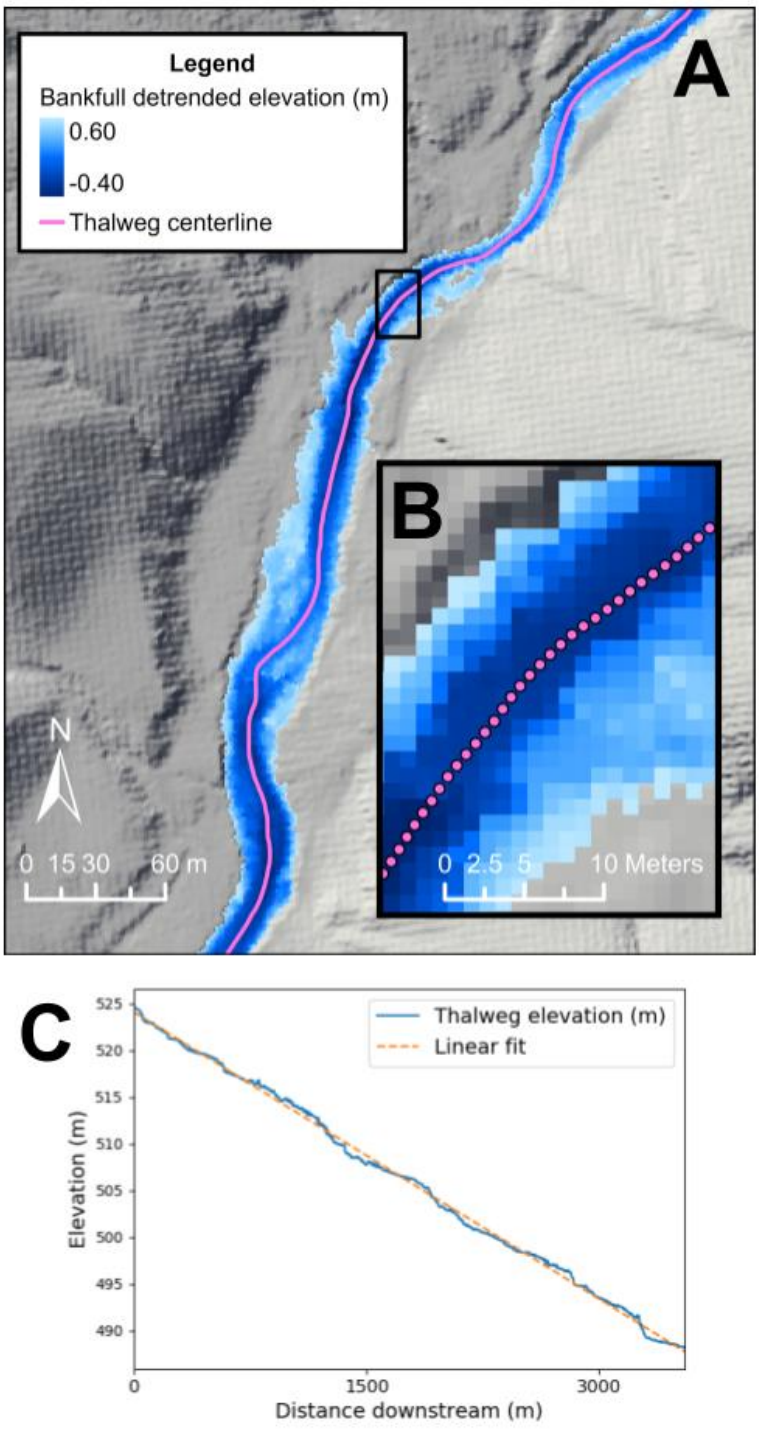

Figure 6. The detrended DEM clipped to the bankfull wetted area, overlaid on a non-detrended hill shade DEM (A), of a partly confined, riffle-pool reach (river type 5). Shown as well are the 0.3 m spaced thalweg elevation sampling points (B), as well the corresponding longitudinal elevation profile and its linear regression fit (C).

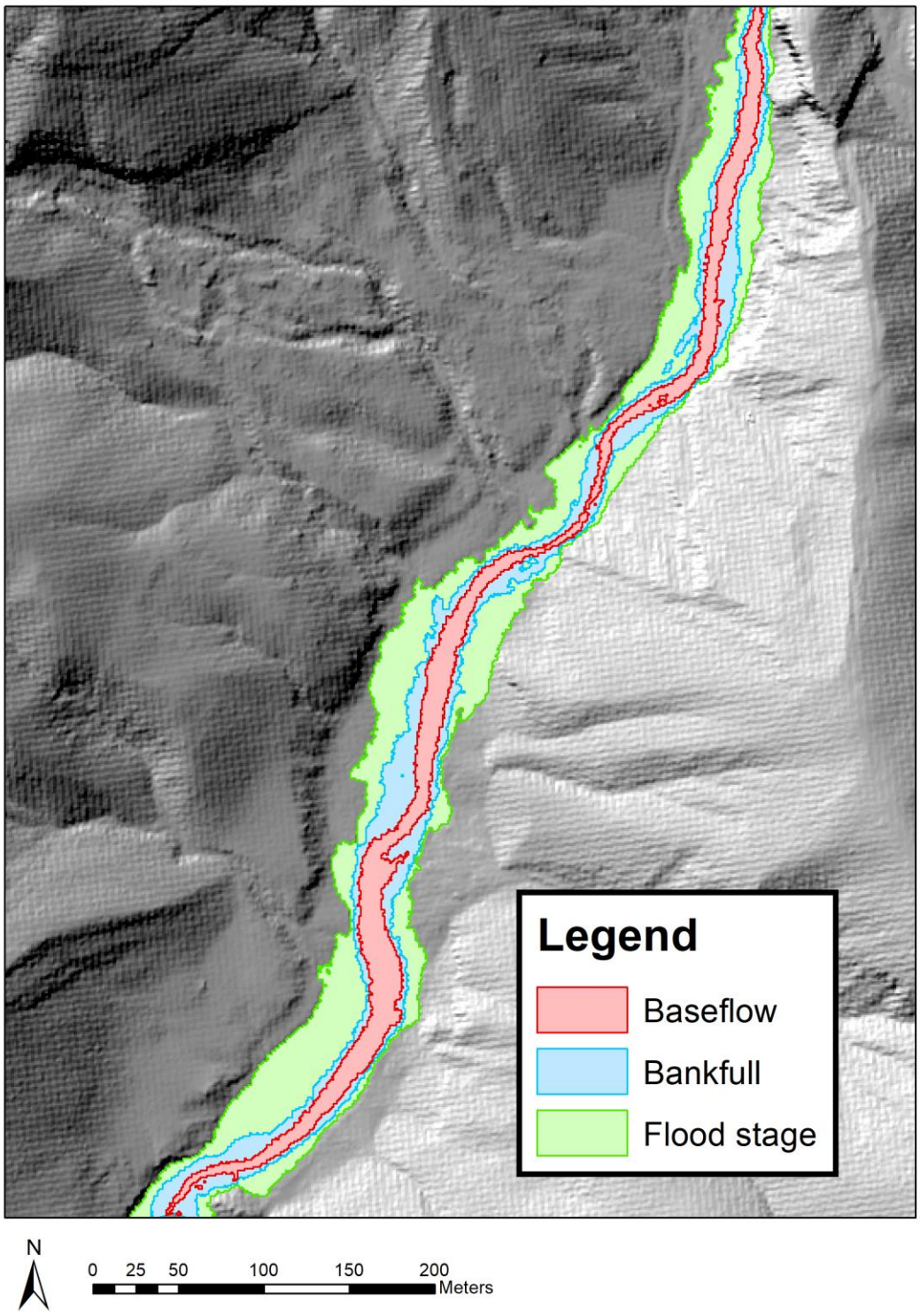

Figure 7. An example of delineated key Zd stages for a partly confined, riffle-pool river reach (River type 5, River ID: 17585756, see supplementary materials).

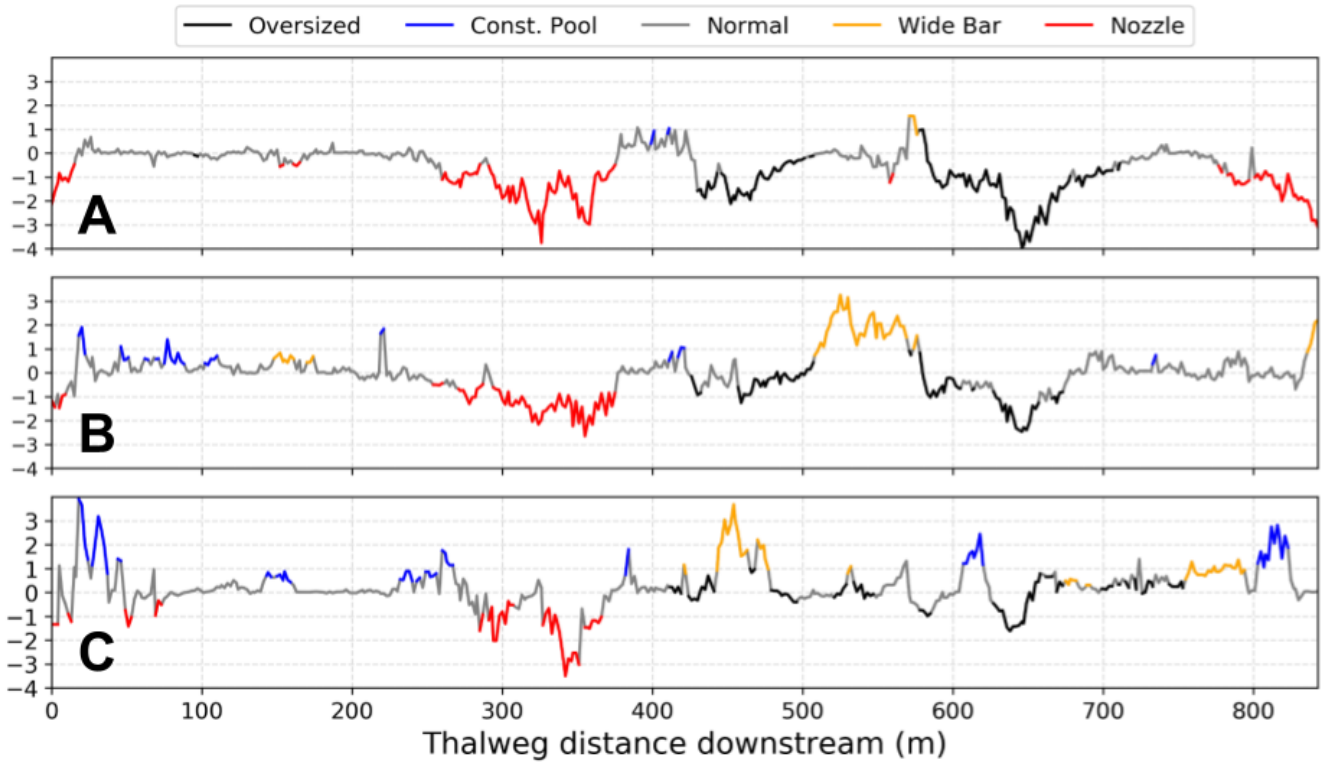

Figure 8. An example of C(Ws, Zs) series at baseflow (A), bankfull (B), and flood-stage (C). Positive values represent cross-sections where Ws and Zs have the same sign, while negative values occur when they have opposite signs (see section 1.3). Landform designations are color coded.

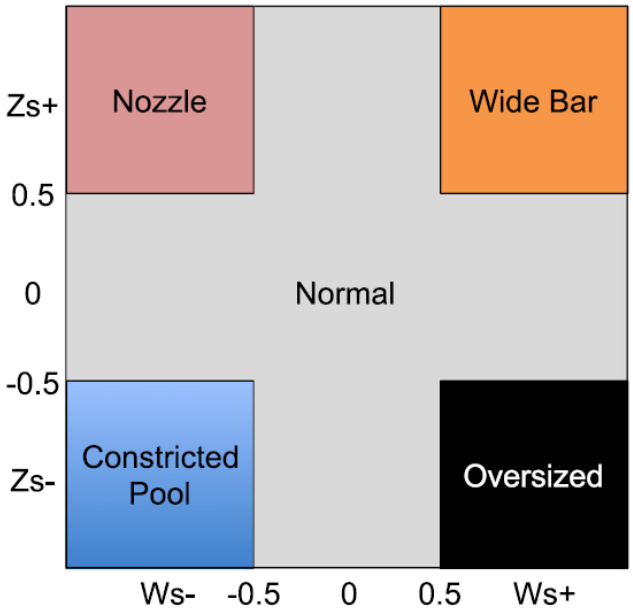

Figure 9. Ws and Zs thresholds for flow-convergence routing landform classification (above). Copied with permission from Pasternack et al. (2018a).

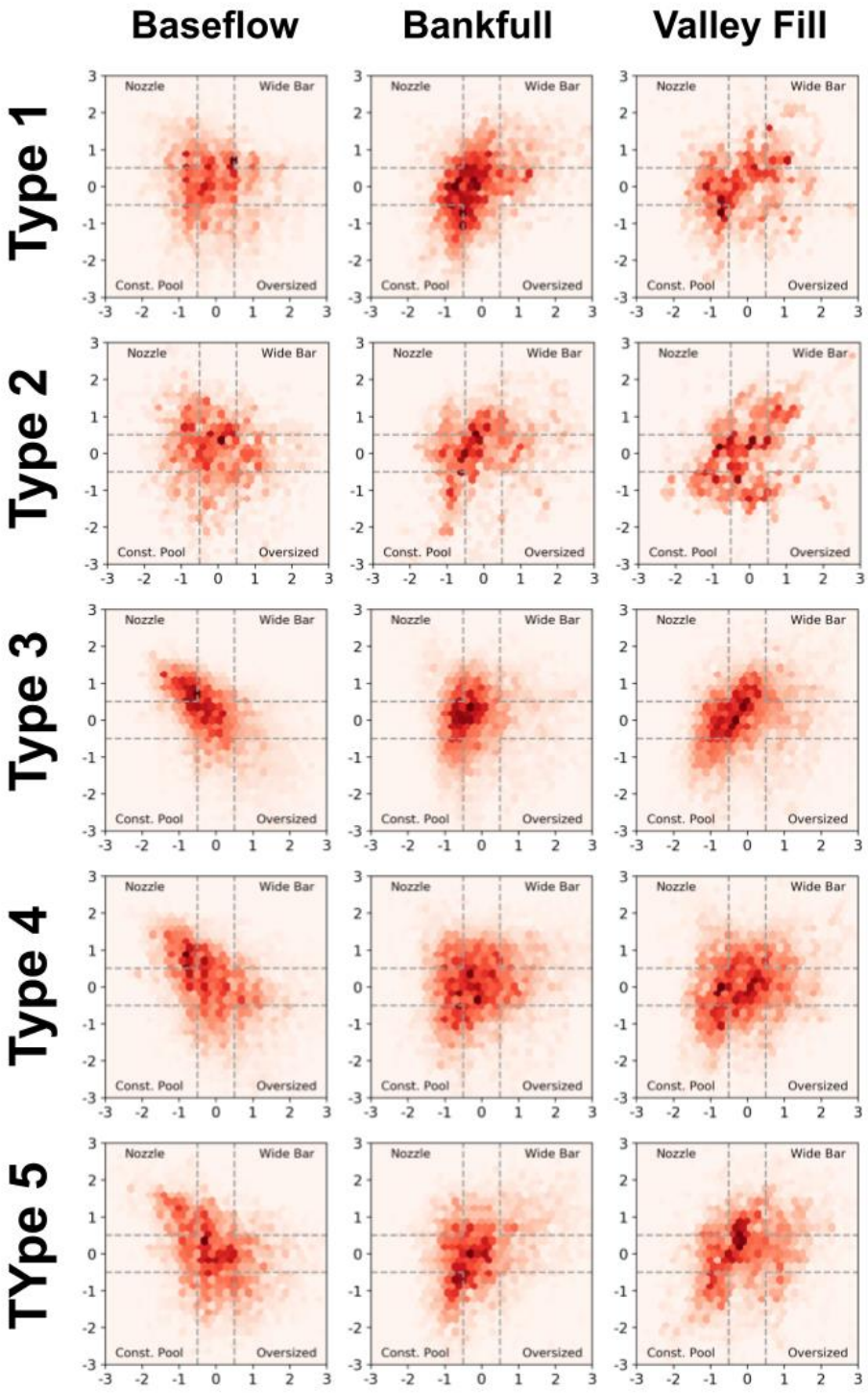

Figure 10. Question O1b. Heat plots showing 2-D distributions of paired cross-section Ws (x-axis) and Zs (y-axis) values. Flow convergence routing landform thresholds are displayed.

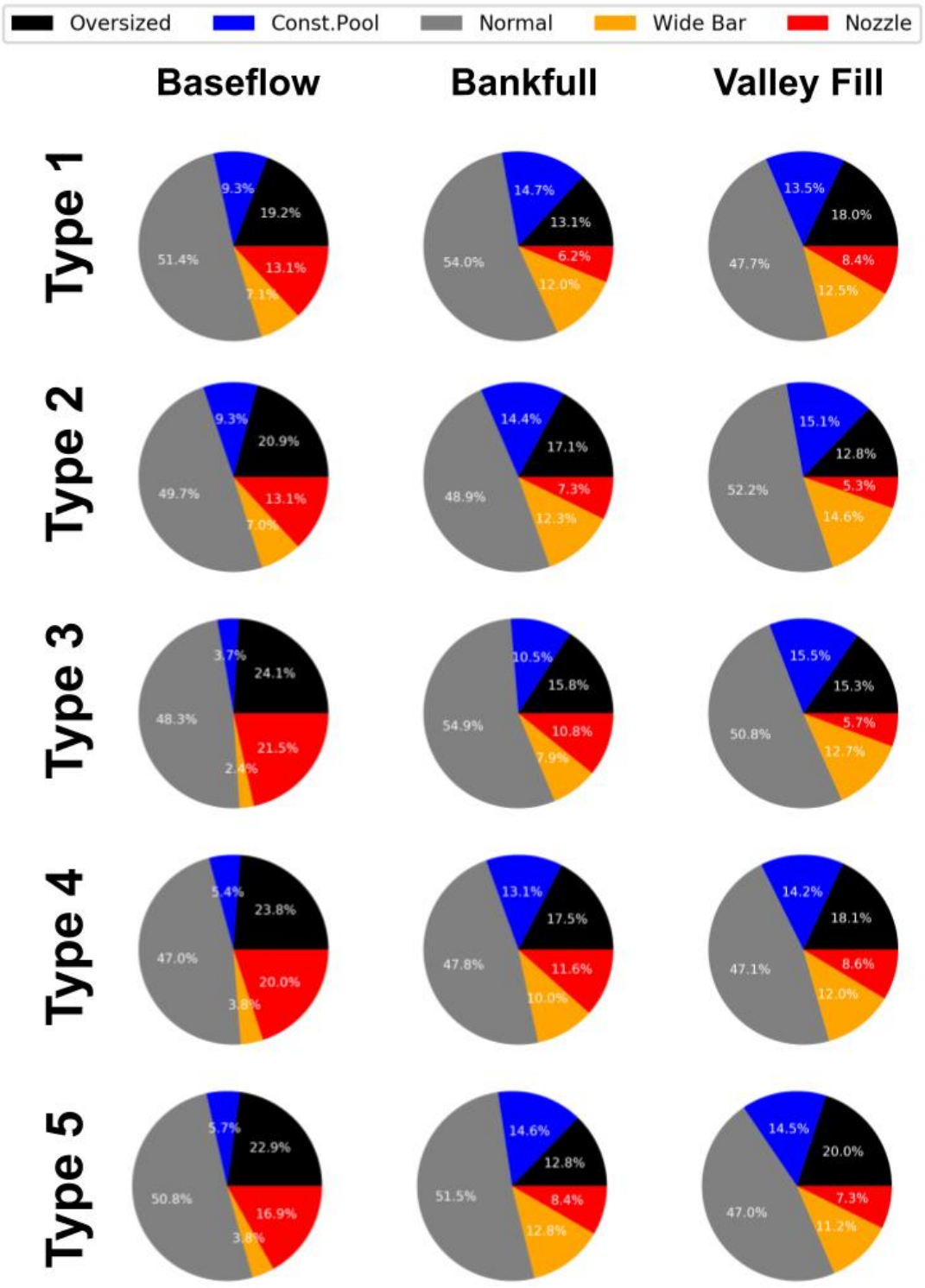

Figure 11. Question O1c. Pie charts showing average relative landform abundance for each river type across flow-stages.

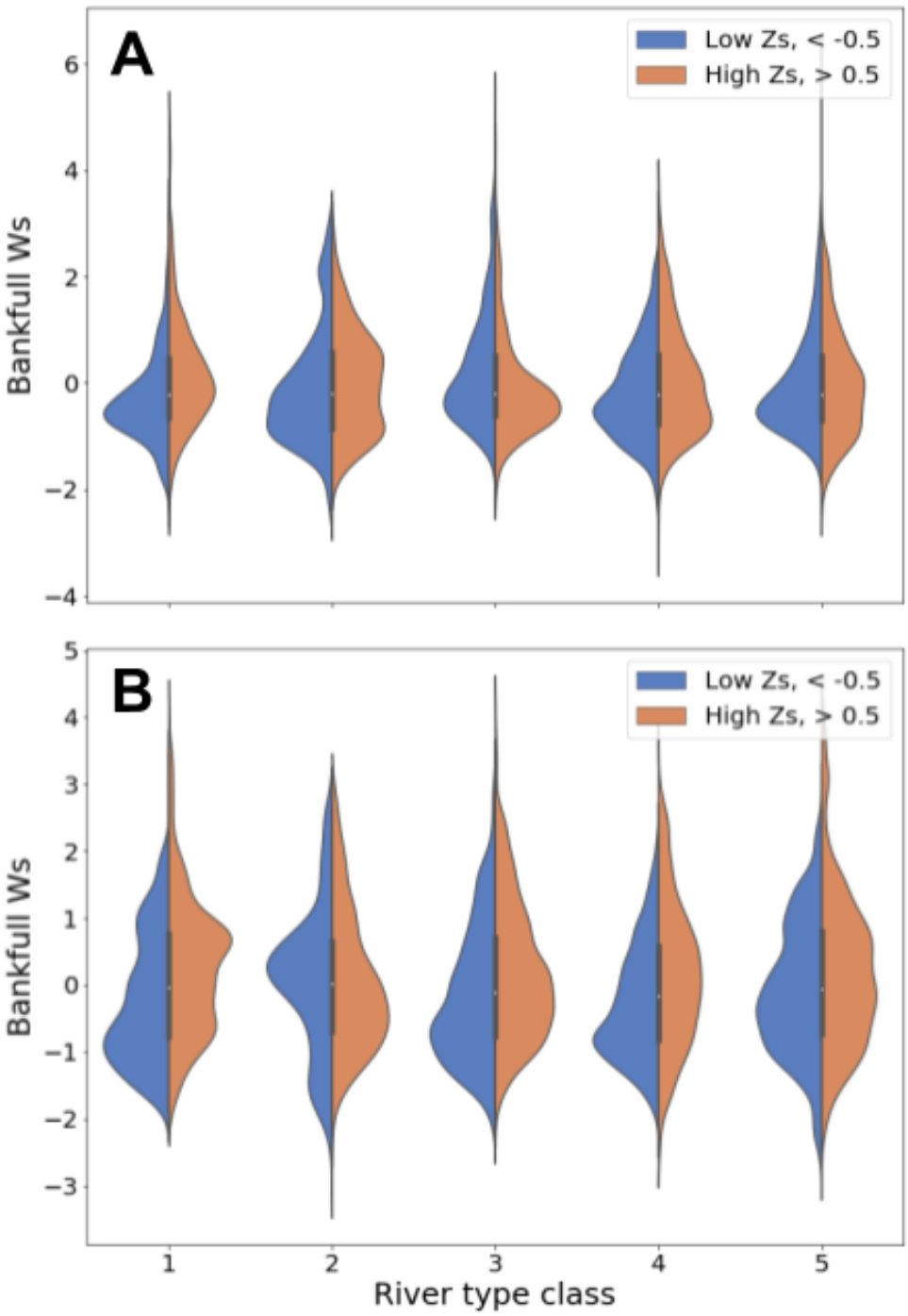

Figure 12. Question O2a. Violin plots showing the distributions of width values at bankfull (A) and flood-stage (B) associated with topographic highs and lows at baseflow and bankfull respectively.

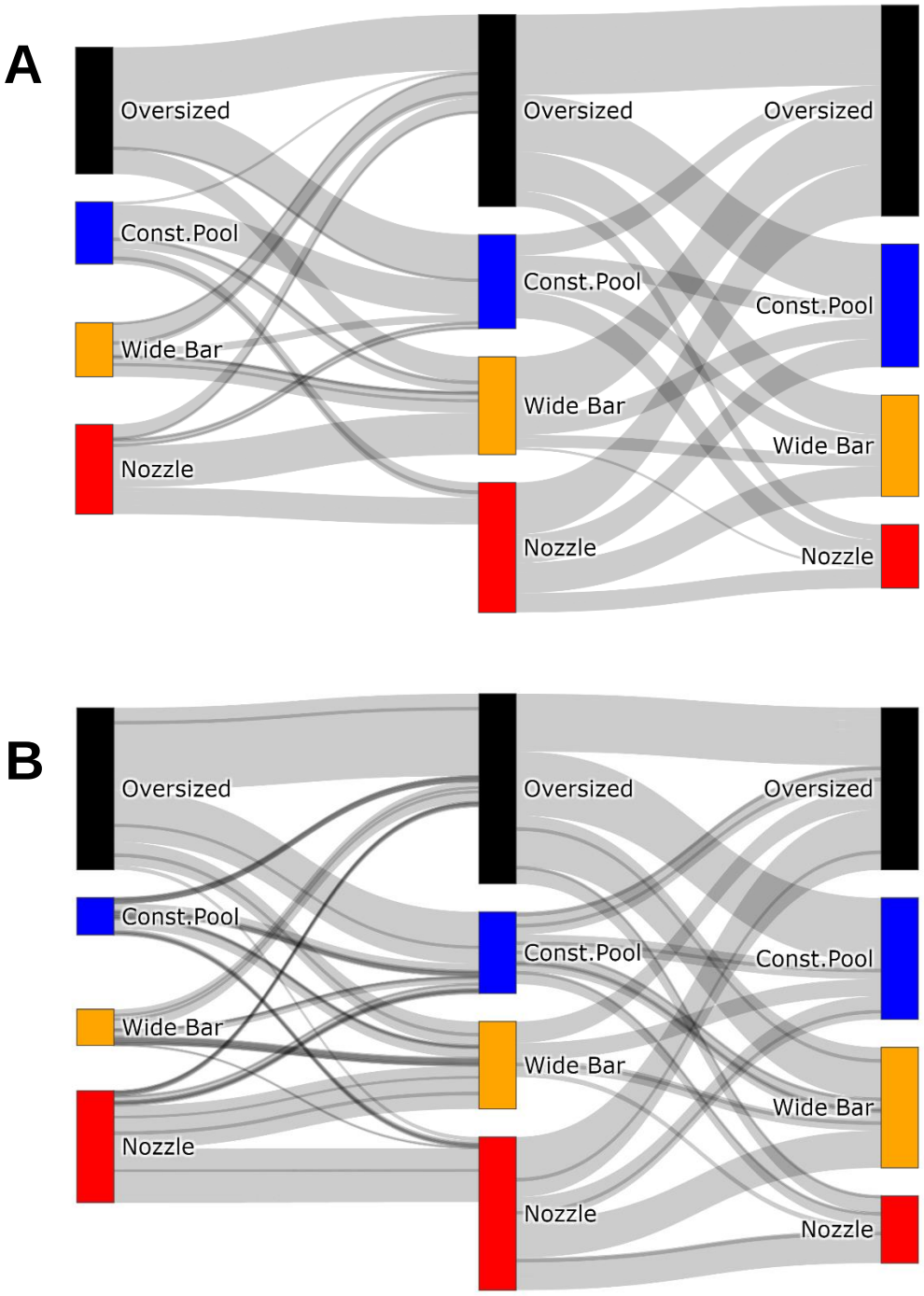

Figure 13. Question O2b. Selected Sankey diagrams visually representing abundances of specific non-normal landforms transitions for river type 1 (A) and 5 (B).